RESEARCH ARTICLE

A stealth adhesion factor contributes to *Vibrio vulnificus* pathogenicity: Flp pili play roles in host invasion, survival in the blood stream and resistance to complement activation

Tra-My Duong-Nu[1,2☯], Kwangjoon Jeong[1,2☯¤], Seol Hee Hong[2,3], Sao Puth[1,2,4], Soo Young Kim[1,2¤], Wenzhi Tan[1,2], Kwang Ho Lee[5], Shee Eun Lee[2,3]*, Joon Haeng Rhee[1,2,3]*

1 Department of Microbiology, Chonnam National University Medical School, Hwasun-gun, Jeonnam, Republic of Korea, **2** Clinical Vaccine R&D Center, Chonnam National University, Hwasun-gun, Jeonnam, Republic of Korea, **3** Department of Pharmacology and Dental Therapeutics, School of Dentistry, Chonnam National University, Gwangju, Republic of Korea, **4** Combinatorial Tumor Immunotherapy MRC, Chonnam National University Medical School, Hwasun-gun, Jeonnam, Republic of Korea, **5** Center for Research Facilities, Chonnam National University, Gwangju, Republic of Korea

☯ These authors contributed equally to this work.
¤ Current address: Vaxcell-Bio Therapeutics, Hwasun-gun, Jeonnam, Republic of Korea
* selee@chonnam.ac.kr (SEL); jhrhee@chonnam.ac.kr (JHR)

Abstract

The tad operons encode the machinery required for adhesive Flp (fimbrial low-molecular-weight protein) pili biogenesis. *Vibrio vulnificus*, an opportunistic pathogen, harbors three distinct *tad* loci. Among them, only *tad1* locus was highly upregulated in *in vivo* growing bacteria compared to *in vitro* culture condition. To understand the pathogenic roles of the three *tad* loci during infection, we constructed single, double and triple tad loci deletion mutants. Interestingly, only the Δ*tad123* triple mutant cells exhibited significantly decreased lethality in mice. Ultrastructural observations revealed short, thin filamentous projections disappeared on the Δ*tad123* mutant cells. Since the pilin was paradoxically non-immunogenic, a V5 tag was fused to Flp to visualize the pilin protein by using immunogold EM and immunofluorescence microscopy. The Δ*tad123* mutant cells showed attenuated host cell adhesion, decreased biofilm formation, delayed RtxA1 exotoxin secretion and subsequently impaired translocation across the intestinal epithelium compared to wild type, which could be partially complemented with each wild type operon. The Δ*tad123* mutant was susceptible to complement-mediated bacteriolysis, predominantly via the alternative pathway, suggesting stealth hiding role of the Tad pili. Complement depletion by treating with anti-C5 antibody rescued the viable count of Δ*tad123* in infected mouse bloodstream to the level comparable to wild type strain. Taken together, all three *tad* loci cooperate to confer successful invasion of *V. vulnificus* into deeper tissue and evasion from host defense mechanisms, ultimately resulting in septicemia.

Author summary

Vibrio vulnificus is so called "flesh eating bacterium" causing fatal sepsis accompanying destruction (necrosis) of soft tissue. The fatal infection occurs after eating contaminated seafood such as oysters or exposure of pre-existing wounds to seawater. Here we show an important bacterial factor that should be used to adhere to human cells and avoid from host immune system. It is very thin thread-like projections from bacterial surface called Tad (tight adhesion) pili. *V. vulnificus* interestingly harbors three Tad gene genetic loci called operons. To understand the roles of the three Tad operons in the pathogenesis, we deleted each of those three gene loci. Employing mouse infection models coupled with molecular genetic analyses, we demonstrate here that all those three Tad operons are cooperatively required for *V. vulnificus* pathogenicity. More specifically, the thin pili threads, hardly observed even under electron microscope, contribute to host cell and tissue invasion, survival in the blood, and resistance to killing activities of serum. These findings explain why *V. vulnificus* has propensity for invading into blood stream from intestine and growing well in the blood resisting against protective immune responses.

Introduction

Vibrio vulnificus is an opportunistic Gram-negative marine pathogen that causes fatal septicemia and necrotizing wound infections in susceptible individuals with underlying hepatic diseases and other immunocompromised conditions. *V. vulnificus* is halophilic and found worldwide in warm coastal and brackish waters in association with shellfish such as oysters and other sea animals. In humans, this pathogen frequently causes rapidly progressing fatal sepsis with a mortality rate of greater than 50% within a few days post-infection after eating raw seafood and contamination of preexisting wounds [1–4]. During the infectious process, *V. vulnificus* must cope with dramatic environmental changes by sensing changes in the host milieu [5]. To establish successful infections *in vivo*, *V. vulnificus* must manage spatiotemporally coordinated changes in the expression levels of various virulence genes.

To understand the genome-wide gene expression changes in *V. vulnificus* after infection, we recently performed a transcriptomic analysis of cells grown *in vivo* using a rat peritoneal infection model. Notably, among the newly identified *in vivo*-expressed genes, a Flp/Tad pilus-encoding gene cluster (the *tad1* locus) was found to be highly upregulated. Flp pili are polymers of the mature Flp pilin protein, and they are assembled and secreted by a complex of proteins encoded by the *tad* operon. Flp pili were reported to be abundantly expressed, extremely adhesive, and bundled in *Aggregatibacter* (previously *Actinobacillus*) [6–9]. The Tad proteins have been reported to be essential for adherence, biofilm formation, colonization, and pathogenesis in a number of genera and are considered to be instrumental in the colonization of diverse environmental niches [6, 7, 10–12].

The genus *Vibrio* includes three main human pathogens (*V. cholerae*, *V. parahaemolyticus* and *V. vulnificus*), all of which were reported to carry genes of pili biogenesis. The type IV pili were most well characterized in pathogenic vibrios and studied for pathogenic roles. The mannose-sensitive hemagglutinin (MSHA) and chitin-regulated pilus (ChiRP), members of the type IV pilus, were reported to contribute to biofilm formation. *V. cholerae* toxin co-regulated pilus (TCP) is critical for host colonization and serves the cognate receptor for cholera toxin (CTX) phage [13–15]. The Flp subtype pilus related to the TCP is associated with the tight

adherence (Tad), from which the gene locus name originated [16]. Homologs of the *tad* locus are widely distributed in the Vibrionaceae and many *Vibrio* genomes encode multiple *tad* loci [17].

V. vulnificus CMCP6 harbors three distinct *tad* loci [18] (S1 Fig), among which the *tad1* locus has been identified as a possible virulence factor because of its ubiquity in sequenced virulent *V. vulnificus* strains [19–21]. The *tad1* expression was preferentially induced under iron-rich conditions [18], whilst the *tad3* locus was expressed in artificial seawater [22]. Recently, through transposon (Tn) insertion mutation analysis, the *tad2* locus (VV2_0084 to VV2_0095) was reported to be important in initial surface attachment, auto-aggregation and resistance to mechanical clearance of bacterial biofilms [12]. However, the pathogenic roles of Tad pili have not yet been addressed for Vibrionaceae. This study attempted to investigate the contribution of the high *in vivo* expression of the *tad1* operon to the *V. vulnificus* pathogenicity and to understand why three similar *tad* operons were maintained throughout the long history of evolution. We evaluated how each *tad* operon contributes to *V. vulnificus* virulence. Since the three *tad* operons share genes with similar function, single-gene-mutation analyses could not rule out overlapping functions of the remaining genes in the same operon or in the other *tad* operons. Thus, we constructed mutant strains with single and multiple complete *tad* loci deletions and then complemented them with individual cosmid clones harboring each *tad* operon. Using a variety of mouse infection models coupled with molecular genetic analyses, we demonstrate here that all three *tad* operons are required for *V. vulnificus* pathogenicity as the cryptic pili contribute to host cell and tissue invasion, survival in the blood, and resistance to complement activation.

Results

Transcriptional analyses of the three structural *flp* genes in *V. vulnificus* infecting the rat peritoneal cavity

To understand how host signals modulate *tad* operon expression in *V. vulnificus*, we analyzed the *in vivo* transcriptional levels of three structural *flp* genes using a rat peritoneal infection model. Real time RT-PCR results indicated a significantly higher *flp-1* mRNA level when the bacteria were grown *in vivo*, corresponding to an approximately 878-fold increase (Fig 1A) ($P < 0.001$). Conversely, both the *flp-2* and *flp-3* transcript levels were slightly decreased when *V. vulnificus* was grown *in vivo* (Fig 1A) ($P < 0.05$ for *flp-2* and $P < 0.001$ for *flp-3*). The expression levels of the *flp* genes were also measured using conventional RT-PCR. Using different numbers of amplification cycles, we confirmed that the *flp-2* and *flp-3* genes were transcribed at low levels under both tested conditions; in particular, *flp-2* expression was detected only after 35 cycles (Fig 1B).

In a wide variety of bacteria, type IV pili expression is solid-surface dependent [23, 24], and the *tad1* locus was recently found to be expressed under iron-limited conditions [18]. Thus, we measured the expression of the *flp-1* gene under these growth conditions. As shown in Fig 1C and 1D, both the iron-limited and surface-associated growth conditions clearly stimulated *flp-1* transcription, increasing its expression levels by approximately 131- and 210-fold, respectively ($P < 0.001$ compared to that of the expression level in HI broth). Combining these two conditions significantly increased the *flp-1* transcript level by 367-fold ($P < 0.01$), but the transcription level was still much lower than that observed *in vivo*. This finding indicates that changing one or two growth parameters in culture does not mirror the *in vivo* environment, where multiple host factors and growth conditions would simultaneously influence *tad1* operon expression.
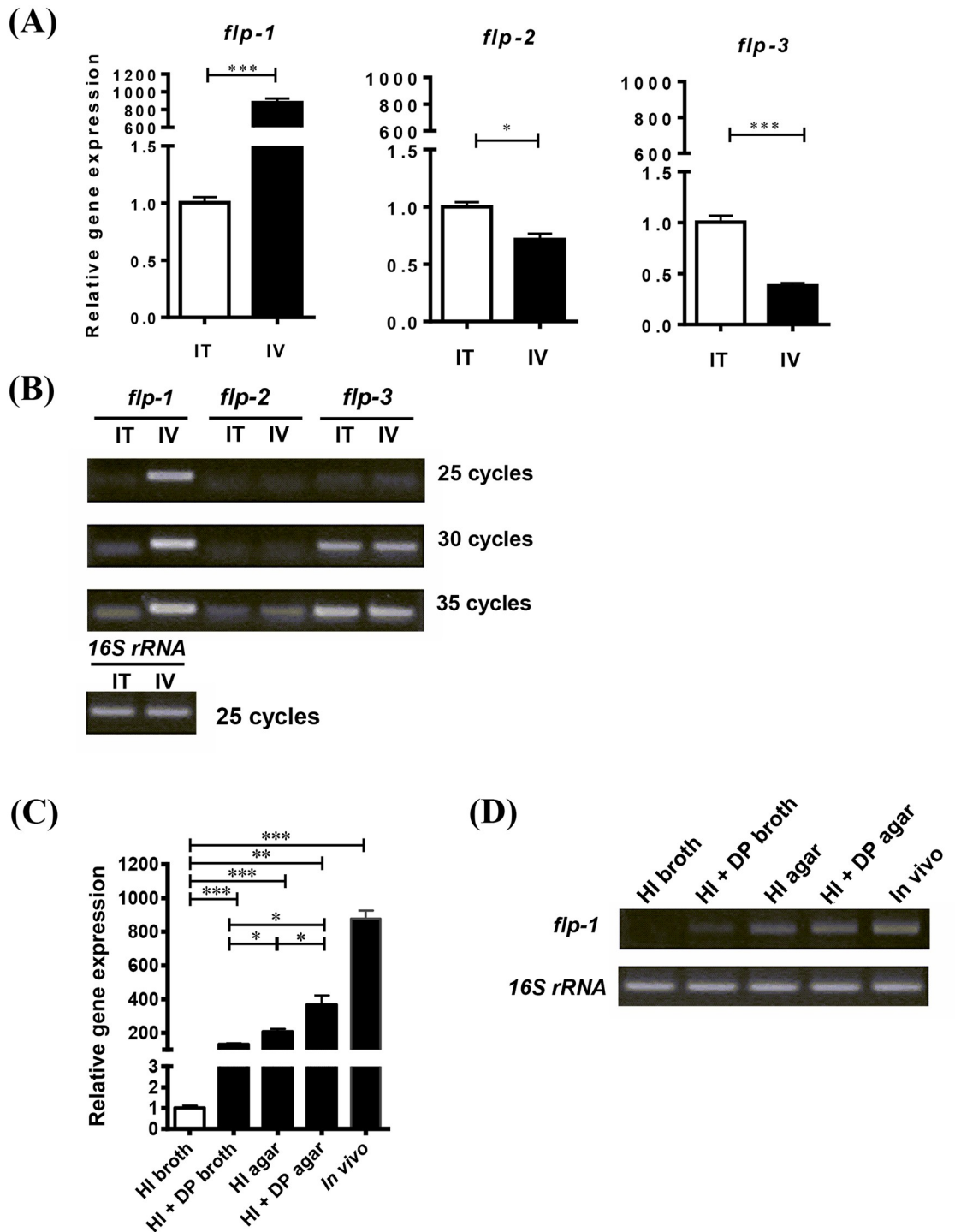
Fig 1. Transcriptional analyses of structural *flp* genes in three *tad* operons of *V. vulnificus*. RNA was isolated from bacteria grown in the rat peritoneal cavity (IV, *in vivo*) or in 2.5% NaCl HI broth (IT, *in vitro*) and the transcript levels of the structural *flp* genes were analyzed via real-time **(A)** and conventional RT-PCR **(B)**. RNA was isolated from bacteria grown under 2.5% NaCl HI broth, iron-limited, solid surface and *in vivo* conditions and the transcript levels of the structural *flp* genes were analyzed via real-time **(C)** and conventional RT-PCR **(D)**. DP (80 μM) was added to 2.5% NaCl HI broth for iron limitation. The real-time RT-PCR data were normalized to *gyrA* and expression relative to the *in vitro* level. Data shown represent the mean ± SEM of three independent experiments performed in triplicate. Statistical analysis was carried out using Student's *t* test (*, $P < 0.05$; ***, $P < 0.001$).

All three *tad* operons are required for full *V. vulnificus* virulence

To explore the contribution of each *tad* operon to *V. vulnificus* pathogenicity, we performed mouse lethality assays employing intraperitoneal (i.p.) and intragastric (i.g.) infection routes. Interestingly, in the i.p. infection model, the Δ*tad123* mutant showed a 41-fold increase in the LD$_{50}$, while the single and double mutants showed no differences (Table 1). Significantly prolonged survival was observed in the Δ*tad123* mutant-administered mice, which received infectious doses of 1.0×10^7 and 1.0×10^6 CFU/mouse. At a dose of 10^7 CFU/mouse, all of the mice infected with wild-type cells died within 5 hours post-infection, whereas approximately 60% of the mice infected with the Δ*tad123* mutant survived up to 48 h after the challenge (S2 Fig) ($P < 0.01$). However, after i.g. infection, which leads to slower translocation of the bacteria into blood circulation, we observed only a 10-fold LD$_{50}$ increase (Table 1). The lethality varied depending on the route of infection, which influences the rate of bacterial invasion, growth and/or clearance at both the primary infection site and in the blood stream. Taken together, all three *tad* operons must be deleted to significantly ameliorate *V. vulnificus* virulence.

The Δ*tad123* mutant exhibits significantly decreased adhesion to HeLa cells

Since common pili are generally involved in the attachment of bacteria to surfaces in nature, we hypothesized that deletion of the three *tad* operons might influence the adhesive ability of *V. vulnificus*. To test this hypothesis, we performed an adhesion assay in which HeLa cells were infected with *V. vulnificus* at an MOI of 250 followed by quantification of the number of bacteria adhered to the host cells. After incubation for 45 min, the number of Δ*tad123* mutant cells adhered to the HeLa cells was 15-fold less than that of the parental wild-type strain (Fig 2A) ($P < 0.001$). The wild-type strain formed small clusters of aggregated bacteria on the surfaces of the HeLa cells, eventually leading to cell lysis. In contrast, only a few Δ*tad123* mutant cells attached to the surfaces of the HeLa cells, and the infected host cells maintained cell contours similar to those of the uninfected cells. However, the adhesion of Δ*tad123* mutant cells to the host cells gradually increased in a time-dependent manner (Fig 2B, $P < 0.01$). The Δ*tad1* mutation played a dominant role in the inhibition of *V. vulnificus* adhesion to host cells (S3A Fig). Complementation with the *tad1*, *tad2* or *tad3* operon (S4 Fig) significantly rescued the adhesive ability of the Δ*tad123* mutant cells (Fig 2A) ($P < 0.001$ for *tad1*, *tad2* and *tad3*).

Structure of the Tad pili on the surface of *V. vulnificus* cells

To observe the morphology of the Tad pili, we prepared *in vivo* grown wild-type, Δ*tad123*, and Δ*tad123* cells carrying pLAFR3::*tad1* locus then performed scanning electron microscopy

Table 1. Effect of the mutation of *tad* operons on the lethality for mice.

V. vulnificus strains	LD$_{50}$ (95% confidence limits)	
	Intraperitoneal infection	**Intragastric infection**
WT	5.5×10^5	1.1×10^5
Δ*tad123*	2.3×10^7	1.1×10^6
Δ*tad1*	2.1×10^5	
Δ*tad2*	5.5×10^5	
Δ*tad3*	4.0×10^5	
Δ*tad12*	5.5×10^5	
Δ*tad13*	7.0×10^5	
Δ*tad23*	6.4×10^5	
Fold increase (WT *vs* Δ*tad123*)	41	10

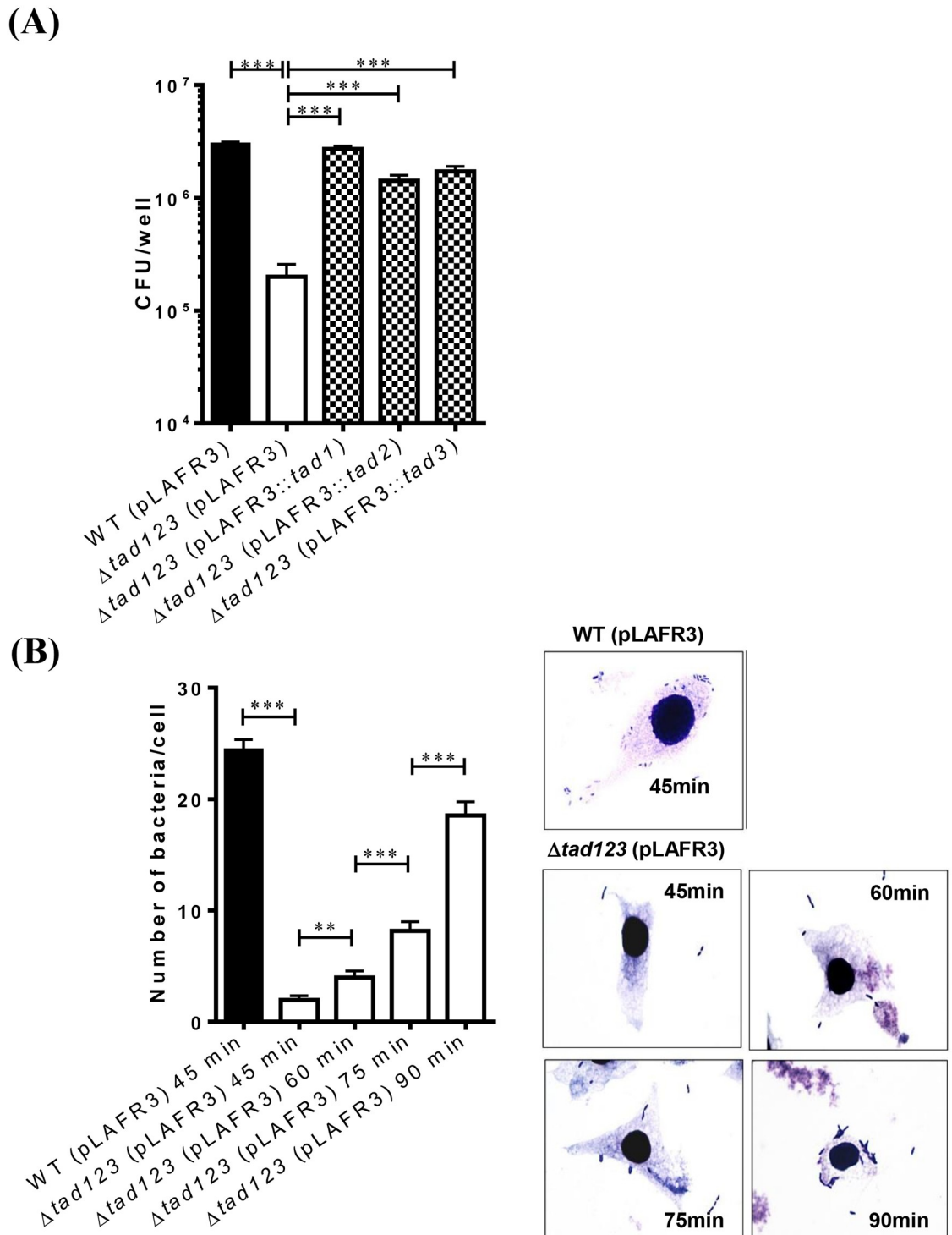https://doi.org/10.1371/journal.ppat.1007767.t001

(A)

(B)

Fig 2. Significantly decreased adhesion to host cells by the Δtad123 mutant (A) and time-dependent recovery (B). HeLa cells were treated with log-phase *V. vulnificus* cells at an MOI of 250 bacteria in the presence of 2 μg/ml tetracycline, and the bacterial cells that adhered to HeLa cells were counted at appropriate time points. The morphology of the infected HeLa cells was observed after Giemsa staining at ×1,000 magnification. Data shown represent the mean ± SEM of five independent experiments performed with six **(A)** or seventeen to forty-four replicates **(B)**. WT (pLAFR3), wild type harboring pLAFR3; Δtad123 (pLAFR3), Δtad123 mutant harboring pLAFR3; Δtad123 (pLAFR3::tad1), Δtad123 mutant *in trans* complemented with pLAFR3::tad1 locus; Δtad123 (pLAFR3::tad2), Δtad123 mutant *in trans* complemented with pLAFR3::tad2 locus); Δtad123 (pLAFR3::tad3), Δtad123 mutant *in trans* complemented with pLAFR3::tad3 locus. Statistical analysis was carried out using Student's *t* test (**, $P < 0.01$).
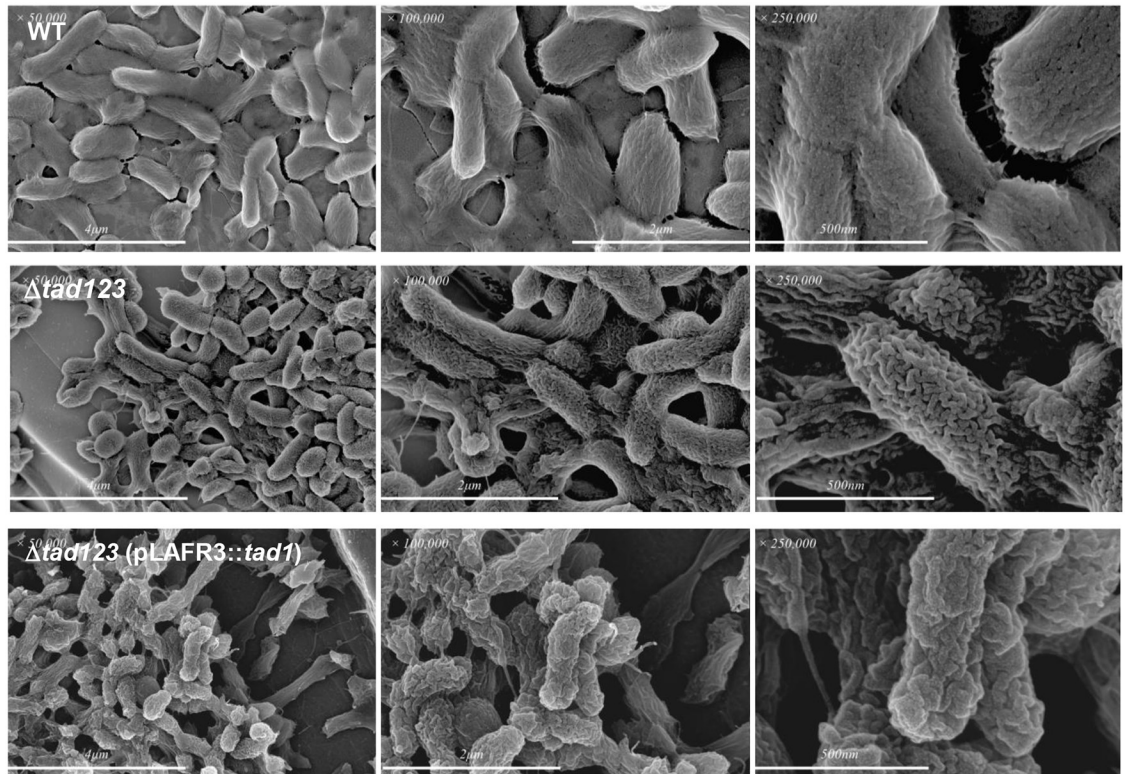
Fig 3. Ultrastructural observation of *V. vulnificus*. Bacteria were grown *in vivo* using a rat peritoneal infection model. The specimens were examined by SEM.

(SEM) observation (Fig 3). In the wild-type strain, the cell surface appeared to be covered with slime-like material. Corrugated elevations and grooves ran along the longitudinal axis. In the *Δtad123* mutant strain, which was devoid of the slime-like materials, the grooves and elevations were more conspicuous compared with those of the isogenic wild-type strain. Moreover, the directionality of the convexity of the surface structure was absent on the mutant surface. Interestingly, the cell surfaces of the *in trans tad1* complemented strains showed similar structural characteristics to the wild type strain, suggesting that the Tad pili contribute to the formation of the slime-like surface structure. However, the typical surface groove and convexity was less obvious in the complemented strains. These results suggest that the Tad pili of *V. vulnificus* might also contribute to the cell envelops biogenesis by including the slime-like outer structure.

We tried to further characterize the thin fimbrial projections of the putative Flp pili via immunogold electron microscopy. Firstly, we produced recombinant Flp pilin proteins and attempted to raise specific antibodies against them in animals. However, we could not obtain any appreciably immunogenic antisera even after many repeated trials. Peptide-based immunizations were also unsuccessful in raising specific antibody responses. We came to conclude that the Flp pilin have very low immunogenicity. To solve this problem, we constructed *V. vulnificus* strains carrying a pBAD24::FlpV5 plasmid expressing a hybrid protein of Flp pilin fused to the highly immunogenic V5 tag (S5 Fig) with the expectation that the plasmid-encoded FlpV5 subunits would assemble into growing pilus fibers under the control of an arabinose-inducible promoter. By using dot blot analysis with an anti-V5 antibody, we confirmed V5-positive signals in the wild type *V. vulnificus* transconjugants (WT-FlpV5) under
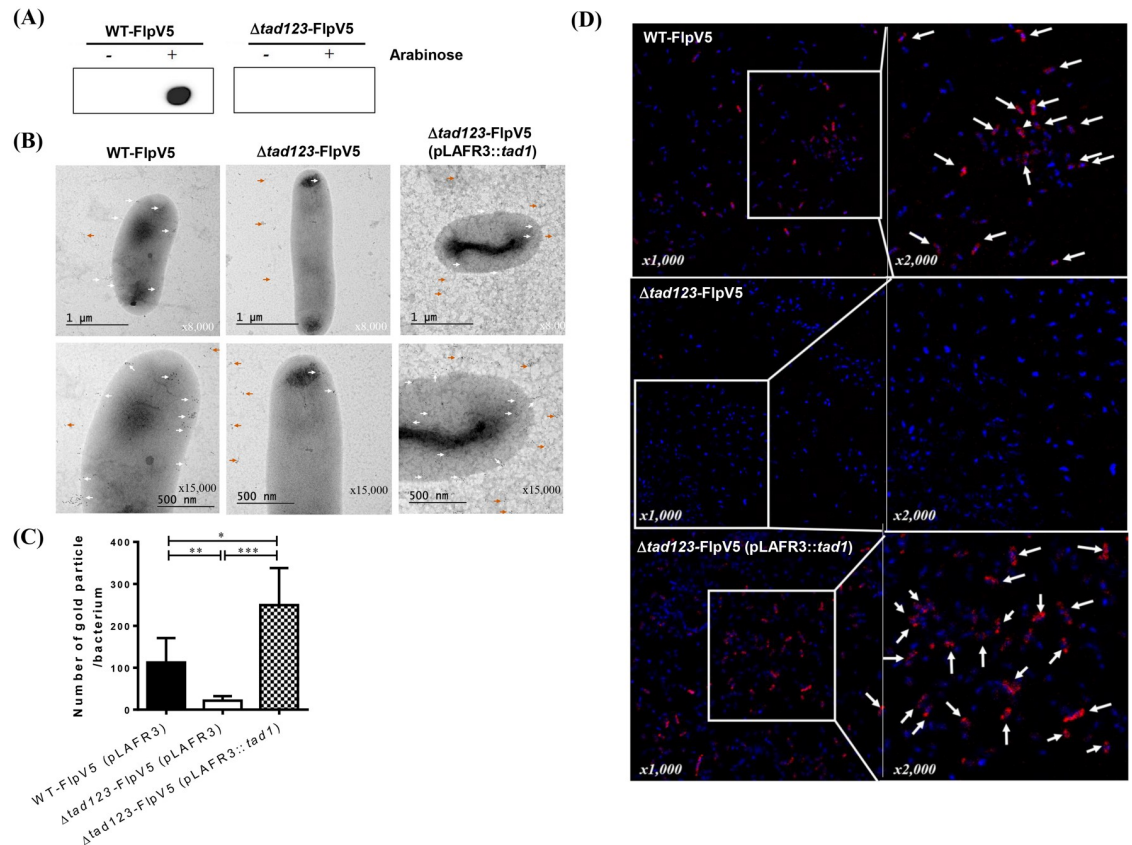
Fig 4. Detection of V5-tagged Flp. (A) Dot blot analysis. Bacteria were grown on a 2.5% NaCl HI-Amp agar plate supplemented with (induced) or without (non-induced) 0.1% arabinose for 4 h. The Flp-V5 fusion protein was detected using an anti-V5 polyclonal antibody. Δ*tad*-FlpV5 indicates the Δ*tad123* mutant strain carrying pBAD24 expressing the Flp-V5 fusion protein, and WT-FlpV5 indicates the wild-type strain carrying pBAD24 expressing the Flp-V5 fusion protein. **(B)** Immunogold labeling and TEM analysis. Bacteria were fixed and incubated with an anti-V5 polyclonal antibody and a 5-nm colloidal gold conjugated goat anti-rabbit IgG secondary antibody. Only *V. vulnificus* cells expressing the Flp-V5 fusion protein showed positivity for immunogold particles on the cell surface. **(C)** A quantification of immunogold particles. The number of immunogold particles were determined from the representative 5 bacterial cells per group under x10,000 magnification. Data shown represent the mean ± SEM. Statistical analysis was carried out Student's *t* test. *, $P < 0.05$; **, $P < 0.01$. **(D)** Immunofluorescent detection of Flp-V5. Bacterial cells were visualized by staining their DNA with DAPI (blue), and anti-V5 detection appears in red (white arrowheads).

https://doi.org/10.1371/journal.ppat.1007767.g004

the inducing conditions (Fig 4A). The immunogold-labeling analysis revealed that wild-type cells displayed gold particles on their surface (white arrow), indicating expressed FlpV5 pilins assembled into the authentic pili (Fig 4B). However, the transconjugated mutant cells (Δ*tad123*-FlpV5) rarely displayed gold particles and this phenotype was complemented *in trans* by the cosmid harboring the wild-type *tad1* locus (Fig 4B). Interestingly, aggregated gold particles were detected on the grid near bacterial cells (orange arrow), suggesting FlpV5 proteins overexpressed under the arabinose induction did not assemble into pilus structure and exported from the bacterial cells. For quantitative analysis, we enumerated the gold particles associated with 5 bacterial cells per group (total 15 bacteria/group) from representative photos under x10,000 magnifications. The number of gold particles associated with the Δ*tad123* mutant cells was significantly scantier than that of the WT ($P < 0.01$) (Fig 4C). The decreased number of gold particles was significantly rescued by the *tad1* operon complementation ($P < 0.001$) (Fig 4C).

Supporting the results of the immunogold staining, immunofluorescence detection via confocal microscopy also revealed positive fluorescent signals for V5p in the FlpV5-expressing wild-type strain (Fig 4D). In contrast, the Δtad123 mutant cells did not show any fluorescent signals, and this deficiency was complemented *in trans* by cosmids encoding the wild-type *tad1* locus (Fig 4D). Many broken filaments were found in the backgrounds of the EM photos, suggesting detachment of the brittle pilus structures during the sample preparation procedures. Taken together, the EM analyses demonstrated the obvious existence of extracellular Flp structures in wild-type *V. vulnificus* CMCP6.

The Δ*tad123* mutant cells display defective RtxA1 production, leading to delayed cytotoxicity toward HeLa cells

RtxA1 is a crucial cytotoxin involved in cellular damage and necrosis of infected tissues [25–29]. We previously reported that host cell contact is required for RtxA1 production and cytotoxicity [25]. Thus, we speculated that attenuated adherence to host cells should hamper RtxA1 production and consequently attenuate host cell killing and tissue invasion. We performed a Western blot analysis to assess RtxA1 production after HeLa cell infection. The toxin was detected using an anti-GD domain antibody targeting the C-terminal fragment (RtxA1-C; approximately 130 kDa), which is internalized in the host cell cytoplasm [30]. As a result of its impaired ability to maintain contact with its host cells, the Δ*tad123* mutant exhibited significantly lower toxin production compared with that of its parental strain (Fig 5A). RtxA1 was secreted in a time-delayed manner in the mutant cells, and its secretion gradually increased over time. This delay was significantly rescued by the *tad* operon complementation (Fig 5A). We next assessed the cytotoxicity of *V. vulnificus* toward HeLa cells over a time course. As shown in Fig 5B, the Δ*tad123* mutant cells showed significantly delayed cytotoxicity toward HeLa cells ($P < 0.001$), whereas the single and double mutants showed no changes ($P > 0.05$) (S3B Fig). The cytotoxicity of the Δ*tad123* mutant cells approached the wild-type level after 2.5 h of incubation (Fig 5B). To investigate the possibility that this result might have been due to bacterial growth retardation in the HeLa cell culture medium, we examined the growth profiles of test strains in high-glucose Dulbecco's Modified Eagle's Medium (DMEM) (S6 Fig). No growth difference was observed between the wild type and Δ*tad123* mutant strains. This delay in the cytotoxicity was significantly recovered by the *in trans* complementation with either the *tad1* or the *tad3* operons (Fig 5C) in the presence of tetracycline ($P < 0.01$ for *tad1* and $P < 0.001$ for *tad3*). The Δ*tad1* mutation appeared to play the most dominant role in the inhibition of *V. vulnificus* adhesion to host cells (S3A Fig). These findings, together with the LD_{50} results, highlight the significance of the three *tad* operons for the adhesion-related virulence of *V. vulnificus*.

The Δ*tad123* mutation results in decreased biofilm formation

The contribution of each *tad* operon was investigated for the biofilm formation. The Δ*tad123* mutant showed significantly decreased biofilm formation compared with wild type strain ($P < 0.001$) (Fig 6A & 6B). The Δ*tad1* mutation appeared to play the most dominant role in the inhibition of *V. vulnificus* adhesion to host cells (S3C Fig). The biofilm formation defect of the Δ*tad123* mutant was complemented *in trans* by the cosmid harboring each of wild type *tad* loci (Fig 6A & 6B).

Tad pili are essential for intestinal invasion by *V. vulnificus*

Bacterial pili are used to attach to host cells and tissues, and confer invasive competence [16, 31–34]. Furthermore, secretion of the RtxA1 cytotoxin, which is induced by adhesion of the

(A)

(B)

(C)
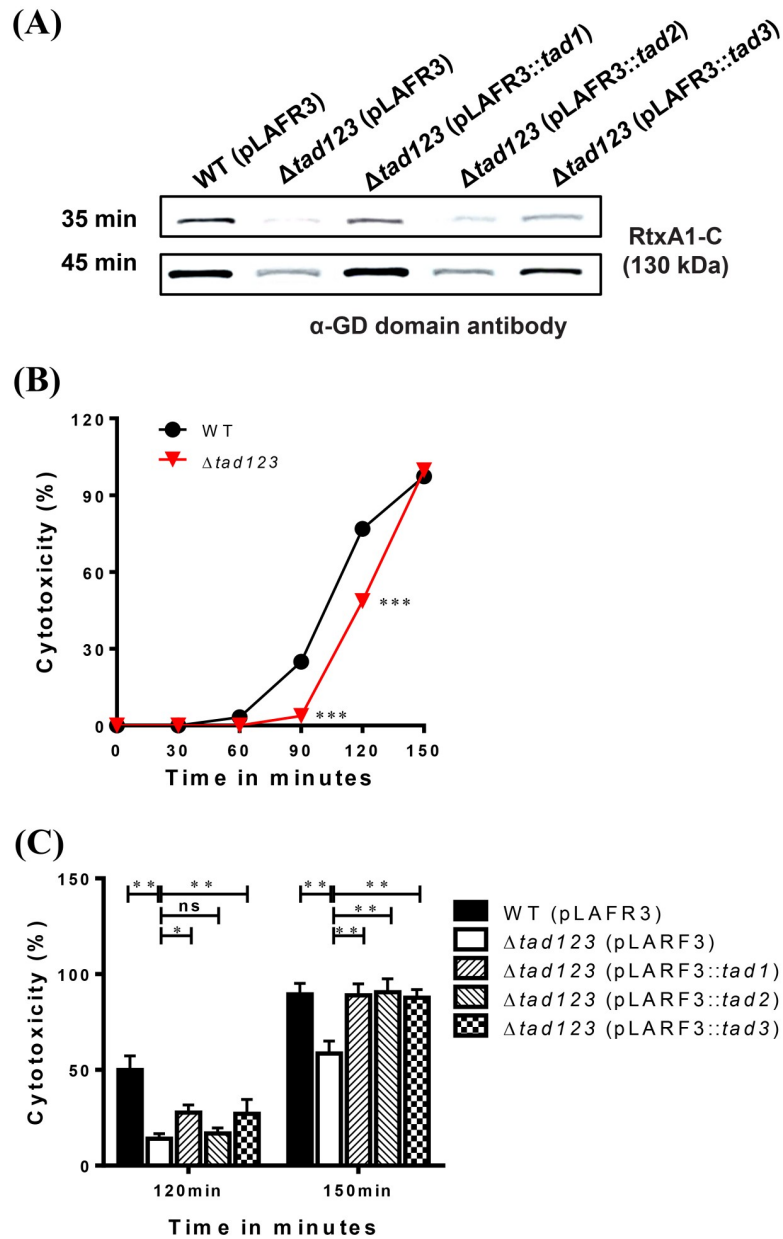
Fig 5. Delayed RtxA1 secretion (A) and cytotoxicity (B) by the Δtad123 mutant cells. (A) For RtxA1 detection, log-phase *V. vulnificus* cells were incubated with HeLa cells in 6-well plates at an MOI of 100 bacteria in the presence of 2 µg/ml tetracycline for 35 or 45 min. The cells in each well were lysed with lysis buffer, followed by concentration using the Amicon Ultra-0.5 centrifugal filter apparatus. The RtxA1 toxin was detected by Western blot analysis using an anti-GD domain antibody (RtxA1-C, a band of approximately 130 kDa). **(B)** Effect of Δtad123 mutations on cytotoxicity against HeLa cells. **(C)** Restoration of cytotoxicity in *tad*-complemented strains in the presence of antibiotics. Data shown represent the mean ± SEM of three independent experiments performed with five replicates. WT (pLAFR3), wild type harboring pLAFR3; Δtad123 (pLARF3), Δtad123 mutant harboring pLAFR3; Δtad123 (pLAFR3::*tad1*), Δtad123 mutant *in trans* complemented with pLAFR3::*tad1* locus; Δtad123 (pLAFR3::*tad2*), Δtad123 mutant *in trans* complemented with pLAFR3::*tad2* locus); Δtad123 (pLAFR3::*tad3*), Δtad123 mutant *in trans* complemented with pLAFR3::*tad3* locus. Statistical analysis was carried out Student's *t* test. **, $P < 0.01$; ***, $P < 0.001$; ns, not significant.

(A)

(B)
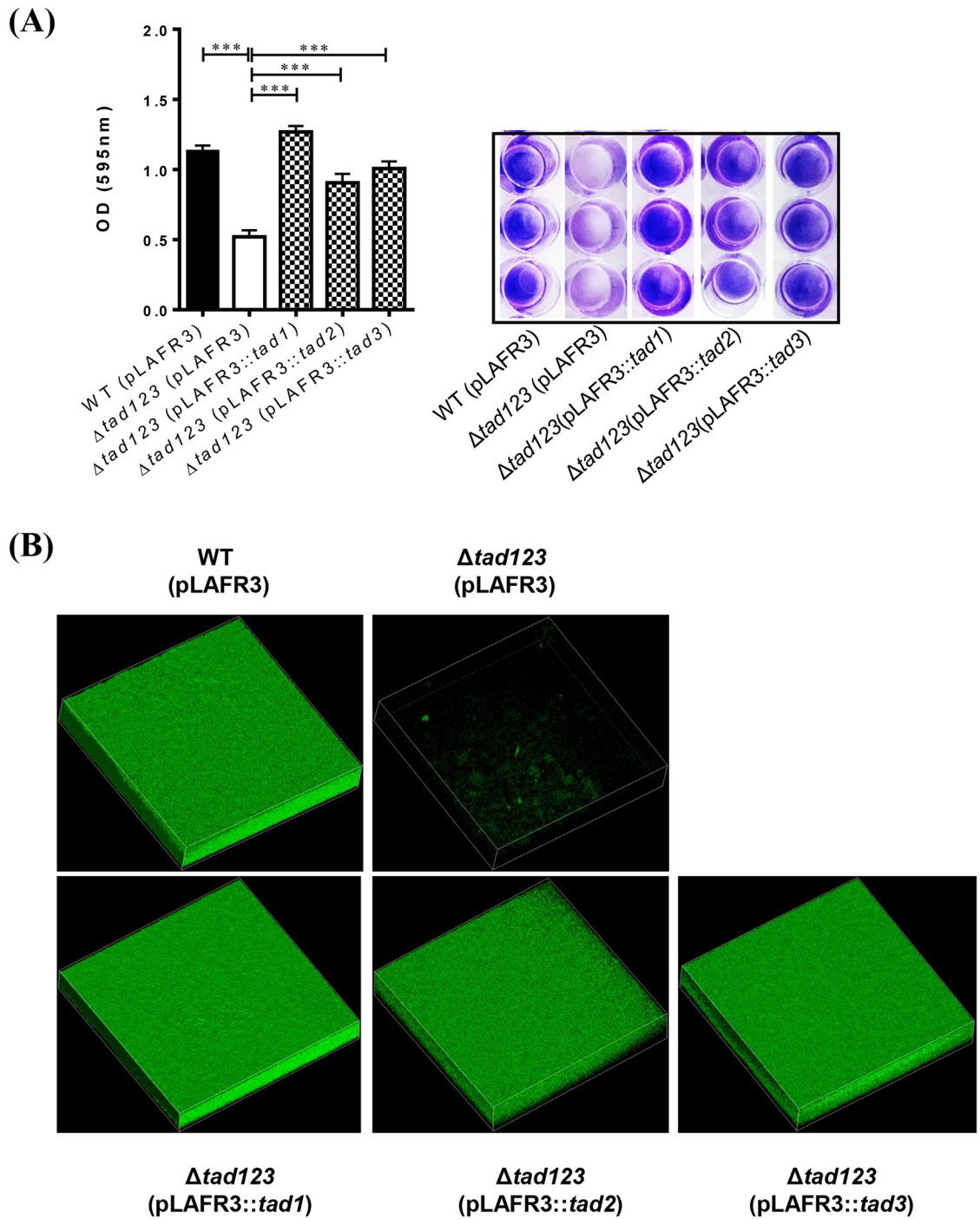
Fig 6. Decreased biofilm formation in the Δtad123 mutant cells. (A) For biofilm formation, log-phase *V. vulnificus* cells (5x10^{5} CFU/ml) was applied into each well of 24 well plate. The plates were further incubated at 37°C for 24 hours. After gentle washing with PBS, the wells were stained with 200 μl of 0.3% crystal violet for 15 min and gently washed with PBS. Data shown represent the mean ± SEM of three independent experiments performed with six replicates. The stained biofilm was extracted with 100% ethanol and diluted (two-fold) with PBS to measure the absorbance at 595 nm. **(B)** Confocal microscopic observation of the acridine orange-stained biofilm. WT (pLAFR3), wild type harboring pLAFR3; Δtad123 (pLAFR3), Δtad123 mutant harboring pLAFR3; Δtad123 (pLAFR3::tad1), Δtad123 mutant *in trans* complemented with pLAFR3::tad1 locus; Δtad123 (pLAFR3::tad2), Δtad123 mutant *in trans* complemented with pLAFR3::tad2 locus); Δtad123 (pLAFR3::tad3), Δtad123 mutant *in trans* complemented with pLAFR3:: tad3 locus. Statistical analysis was carried out using Student's *t* test. ***, $P < 0.001$. WT, wild-type *V. vulnificus*.

bacterial cells to the host cells, is highly correlated with host tissue invasion [25]. To investigate the effects of mutation of the *tad123* loci on *V. vulnificus* invasion, we carried out an *in vivo* invasion assay using a mouse ligated ileal loop infection model. The viable bacterial cells in the blood of the infected mice were quantified to evaluate tissue invasiveness of bacteria. The number of bacterial cells in the blood samples from the Δ*tad123* mutant-infected mice was significantly lower than that in the mice infected with the wild-type strain, even 6 hours post-infection (Fig 7A) ($P < 0.001$).

In addition to the *in vivo* invasion assay, bacterial invasiveness was further confirmed using an *in vitro* intestinal epithelial barrier system. Polarized HCA-7 cells grown on Transwells were apically infected with bacteria, leading to physical apical-to-basolateral trans-epithelial migration of the bacteria. After 3 to 5 hours of incubation, we detected significantly fewer Δ*tad123* mutant cells than wild-type cells in the basolateral chamber (Fig 7B) ($P < 0.05$). The single and double mutants showed no changes (S3D Fig). The cell count of the Δ*tad123* mutant reached that of the wild-type strain after 6 hours of incubation. The defect of trans-epithelial translocation of the Δ*tad123* mutant was complemented *in trans* by the cosmid harboring each of wild type *tad* loci (Fig 7C). Taken together, the *in vitro* data and the *in vivo* invasion results demonstrate a function for Tad pili in conferring invasive competence to *V. vulnificus*.

Tad pili are important for *V. vulnificus* survival in blood

It is likely that the impaired invasion alone could not fully account for the higher LD_{50} observed for the Δ*tad123* mutant in the intraperitoneal infection model (Table 1); therefore we hypothesized that mutation of the *tad123* loci could compromise *V. vulnificus* survival in the bloodstream. To investigate this possibility, we monitored the number of viable bacteria in the blood over a time course following intraperitoneal (i.p.) or intravenous (i.v.) infection. Interestingly, the triple mutant cells were defective at surviving in mouse blood. Significantly fewer mutant cells were recovered from the blood of mice infected via both routes (Fig 8A and 8B). In particular, very few mutant cells were detected after direct introduction of the bacteria into the blood stream via i.v. injection, resulting in an approximately 3-log reduction in the number of CFUs compared with the number of CFUs detected for the wild-type strain (Fig 8A). The viable bacteria in the blood following i.p. infection should represent *V. vulnificus* cells that succeeded at both invasive translocation and resisting the serum bactericidal activities. On the other hand, the i.v. infection model shows how well the wild-type and mutant bacteria survived the serum bactericidal activities. These findings clearly indicate that Tad pili also play important roles in the survival of *V. vulnificus* in the blood stream.

Tad pili are required for *V. vulnificus* serum resistance

Serum bactericidal activity is an important innate immune defense against intravascular invasion by bacterial pathogens [35, 36]. Thus, we hypothesized that Tad pili might play a protective role against serum components. To address this hypothesis, we tested the susceptibility of triple mutant cells to normal human serum (NHS). Bacterial viability was assessed after 2 hours of incubation with different NHS concentrations. Notably, the bacteria lacking all three *tad* loci were extremely sensitive to human serum (Fig 9A). For the Δ*tad123* mutant, 20% NHS led to dramatically decreased viability, and exposure to 40% NHS resulted in 4-log scale decrease of the viable cells. In contrast, the wild-type cells showed resistance against human serum (Fig 9A). A time course assay with 60% NHS was carried out to further compare the serum resistance levels of the isogenic mutant and the wild-type strains. During the first hour of incubation, more than 3-log scale of the Δ*tad123* mutant lost viability (Fig 9B). The
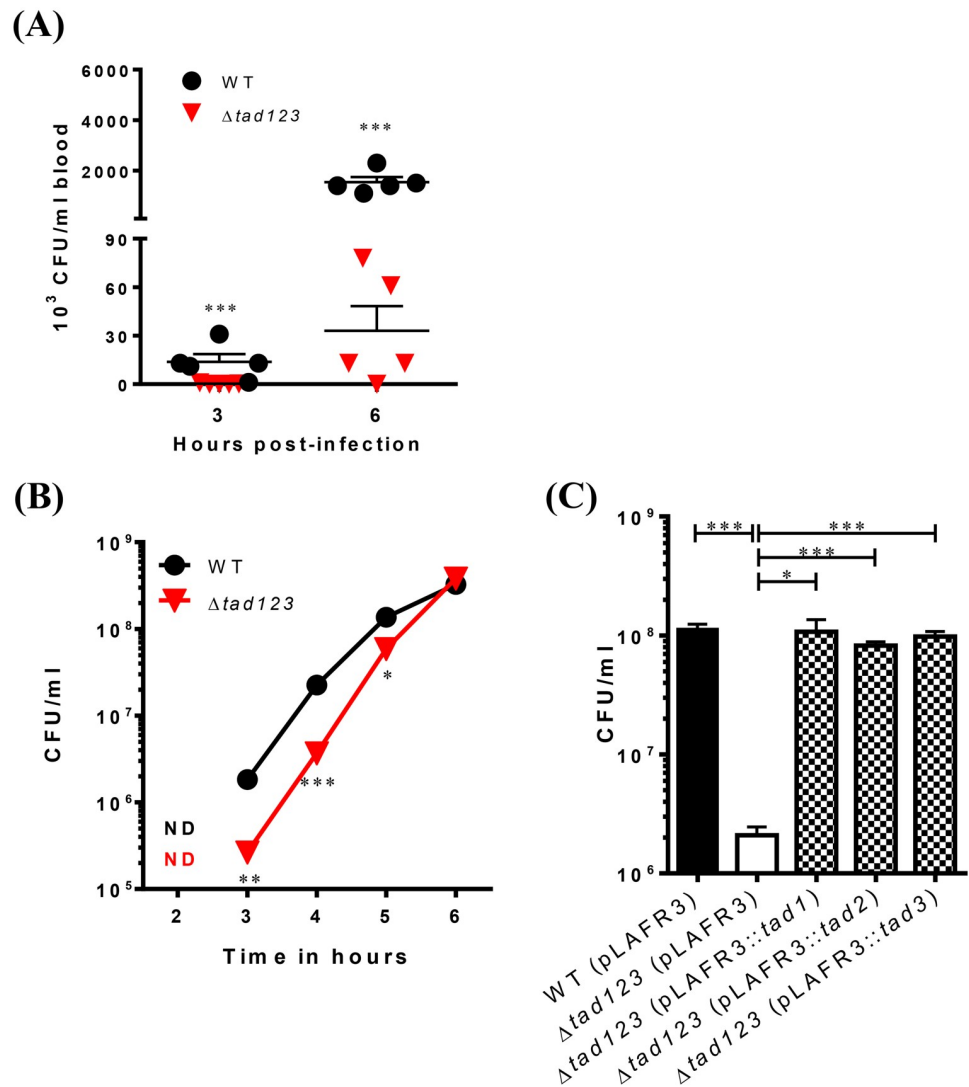
(A)

(B)

(C)

Fig 7. Effect of the triple *tad* operon mutation on *in vivo* and *in vitro* invasion. (A) *In vivo* invasion. Log-phase bacteria were inoculated into ligated ileal loops of mice. Blood samples were acquired from infected mice by cardiac puncture at the indicated times. Viable cells were counted by plating on 2.5% NaCl HI agar plates. Data shown represent the mean ± SEM of three independent experiments performed in five mice. **(B) *In vitro* invasion.** HCA-7 cells grown on Transwell filters were apically exposed to log-phase bacteria. Invasiveness was determined by measuring the number of bacterial cells that translocated from the apical to the basolateral compartment of the Transwells. WT (pLAFR3), wild type harboring pLAFR3; Δ*tad123* (pLAFR3), Δ*tad123* mutant harboring pLAFR3; Δ*tad123* (pLAFR3:: *tad1*), Δ*tad123* mutant *in trans* complemented with pLAFR3::*tad1* locus; Δ*tad123* (pLAFR3::*tad2*), Δ*tad123* mutant *in trans* complemented with pLAFR3::*tad2* locus); Δ*tad123* (pLAFR3::*tad3*), Δ*tad123* mutant *in trans* complemented with pLAFR3::*tad3* locus. Data shown represent the mean ± SEM of three independent experiments performed with triplicates. **(C)** Restoration of *in vitro* invasion in *tad*-complemented strains at 6 h post-incubation in the presence of 2 µg/ml tetracycline. Viable bacterial cells were counted by plating on 2.5% NaCl HI agar plates. Data shown represent the mean ± SEM of three independent experiments performed with triplicates. Statistical analysis was carried out using Student's *t* test. *, $P < 0.05$; **, $P < 0.01$; ***, $P < 0.001$; ND, not detected (detection limit; 1×10^3 CFU/mL).

https://doi.org/10.1371/journal.ppat.1007767.g007

single and double mutants showed no changes (S3E Fig). The serum susceptibility of the Δ*tad123* mutant was complemented *in trans* by the cosmid harboring each of wild type *tad* loci (Fig 9A & 9B). This result explains the significant difference in the survival rates observed between the wild type and Δ*tad123* mutant strains, and further confirms that Tad pili are required for *V. vulnificus* serum resistance.
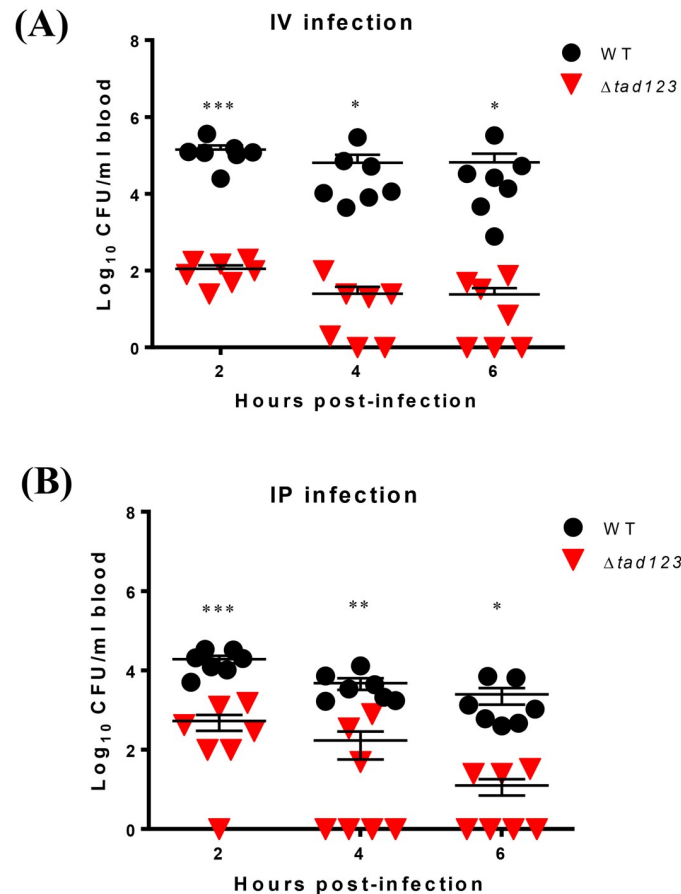
Fig 8. Recovery of *V. vulnificus* from blood after intravenous or intraperitoneal mouse infection. Each mouse was intravenously (**A**) or intraperitoneally (**B**) injected with bacteria that had been previously incubated in the rat peritoneal cavity for 6 hours for *in vivo* adaptation. Blood samples were acquired from infected mice via cardiac puncture at the indicated times. Viable bacterial cells were counted by plating on 2.5% NaCl HI agar plates. Very low numbers of Δ*tad123* mutant cells were recovered from the blood of infected mice. Data shown represent the mean ± SEM of three independent experiments performed in seven mice. Statistical analysis was carried out using Student's *t* test (*, $P < 0.05$; **, $P < 0.01$; ***, $P < 0.001$).

https://doi.org/10.1371/journal.ppat.1007767.g008

The alternative complement pathway plays a dominant role in the killing of the Δ*tad123* mutant cells

Given that the complement system, which is activated by pathogenic bacteria is primarily responsible for the direct killing of bacteria in NHS [37], we further dissected the bactericidal activity of three complement pathways activated by *V. vulnificus*. Indeed, the use of heat-inactivated serum (HIS) lacking the lytic complement activity successfully rescued the viability of the mutant strain (Fig 9C). This finding indicates that heat-labile complement proteins are responsible for the killing of the Δ*tad123* mutant cells in NHS. Complement activation occurs via one or more of three pathways: the classical pathway, the MBL/lectin pathway and the alternative pathway [35]. To identify which complement pathway was responsible for the death of the Δ*tad123* mutant cells in serum, we selectively blocked the specific complement activation pathways. Remarkably, inhibition of the alternative pathway completely ablated the complement-mediated killing activity. The survival of the Δ*tad123* mutant cells fully recovered to the wild-type level in bentonite-absorbed NHS (Fig 9C). Furthermore, inhibition of either
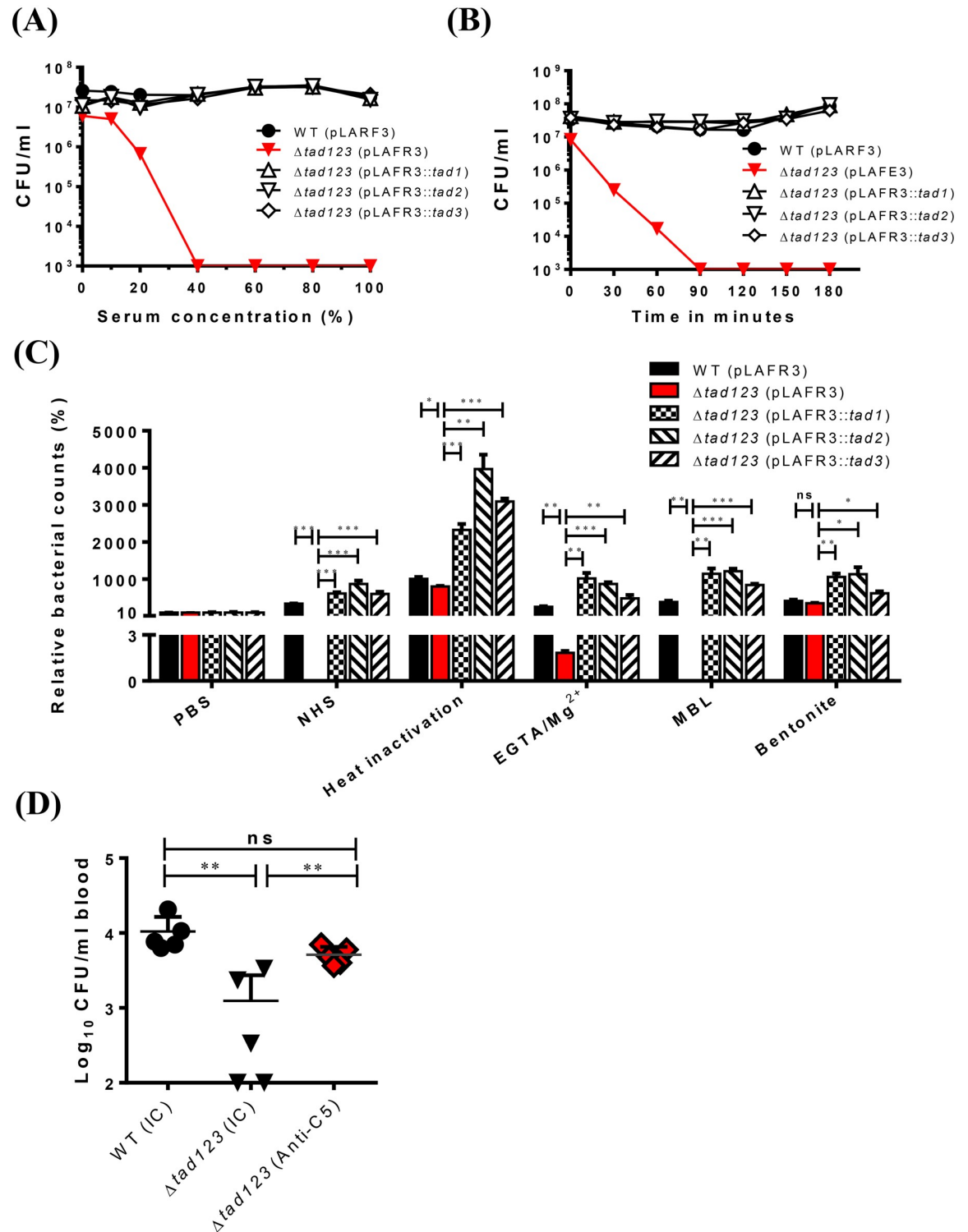
Fig 9. Survival of *V. vulnificus* against human serum bactericidal killing. (A) Log-phase bacteria grown in the presence of 2 μg/ml tetracycline were washed with PBS and then incubated with different NHS concentrations at 37 ˚C for 2 h and the numbers of viable cells were determined. **(B)** Log-phase bacteria grown in the presence of 2 μg/ml tetracycline were washed with PBS were incubated with 60% NHS and the numbers of viable cell were determined in a time-dependent manner. **(C)** Log-phase bacteria grown in the presence of 2 μg/ml tetracycline were washed with PBS were incubated with HIS, undiluted NHS, EGTA/Mg^{2+}-treated NHS, MBL-depleted NHS or bentonite-treated NHS for 2 h. Viable bacterial cells were counted by plating on 2.5% NaCl HI agar plates. Bacteria were incubated in PBS as a control. WT (pLAFR3), wild type harboring pLAFR3; Δ*tad123* (pLAFR3), Δ*tad123* mutant harboring pLAFR3; Δ*tad123*

(pLAFR3::*tad1*), Δ*tad123* mutant *in trans* complemented with pLAFR3::*tad1* locus; Δ*tad123* (pLAFR3::*tad2*), Δ*tad123* mutant *in trans* complemented with pLAFR3::*tad2* locus); Δ*tad123* (pLAFR3::*tad3*), Δ*tad123* mutant *in trans* complemented with pLAFR3::*tad3* locus. Data shown represent the mean ± SEM of four independent experiments performed in triplicates. Statistical analysis was carried out using Student's *t* test (C). ***, $P < 0.001$. ns, non-significant (detection limit; 1×10^3CFU/mL). **(D)** Viable *V. vulnificus* cells in bloodstream of anti-C5 monoclonal antibody pretreated mice. Groups of mice were administered with 40mg/kg mouse anti-C5 two times as described Materials and Methods and then the mice were intraperitoneally infected with 5×10^5 wild type or Δ*tad123* mutant cells previously incubated in the rat peritoneal cavity for 6 hours for *in vivo* adaptation. Blood samples were acquired by eye bleeding. Viable bacterial cells were counted by plating on 2.5% NaCl HI agar plates. Data are shown as the mean ± SEM (n = 5). Statistical analysis was done using Student's *t* test (*, $P < 0.05$; **, $P < 0.01$; ***, $P < 0.001$). IC, isotype control.

the classical pathway or the lectin pathway partially recovered the survival of the mutant cells (Fig 9C). The serum susceptibility of the Δ*tad123* mutant was complemented *in trans* by the cosmid harboring each of wild type *tad* loci (Fig 9C). Taken together, these results indicate that Tad pili likely play an important role in protecting *V. vulnificus* from direct complement-mediated bacteriolysis resulting predominantly from activation of the alternative pathway.

Depletion of mouse complement system support *in vivo* survival of Δ*tad123* mutant

To test whether serum susceptibility of the Δ*tad123* mutant is reverted *in vivo* by inhibition of complement system, we pretreated mice with a specific complement-inhibiting drug (anti-C5 antibody) approved by FDA [38] and then infected the mice with wild type or Δ*tad123* mutant cells. We monitored the number of viable bacteria in the blood in a time course following intraperitoneal infection. As shown in Fig 9D, the viable bacterial count of Δ*tad123* mutant could be rescued by the anti-C5 antibody treatment almost to the level of wild type strain. These data clearly indicate that reduced viability of the Δ*tad123* mutant is due to increased susceptibility to complement system in the mouse infection model. Given the innately lower complement level in mice compared with human [39], the Tad pili system should play more dominant roles in the pathogenesis of human infections.

Discussion

Host-pathogen interactions during microbial infections can be described as a dynamic battlefield where the microbe's clever strategies for survival and multiplication confront the formidable host immune defenses. To investigate the virulence regulation of *V. vulnificus* during infection, we recently performed comparative genome-wide transcriptional analyses of cells grown *in vitro* and *in vivo*. A rat peritoneal infection model was used to simulate the physiological host milieu. Interestingly, among the newly identified *in vivo*-expressed candidate genes, *tad1* was found to be highly upregulated *in vivo* (unpublished data). The pathogenic potential of the *tad1* cluster is also supported by previous reports of the ubiquity of the *tad1* locus in sequenced virulent *V. vulnificus* strains [19–21]. Furthermore, it is notable that the genome of *V. vulnificus* CMCP6 contains three distinct *tad* loci, in which similar functional genes are organized in the same order and transcriptional orientation. In this study, our goals were to investigate why *V. vulnificus* CMCP6 has maintained three *tad* loci throughout evolution and how each *tad* operon contributes to *V. vulnificus* virulence and to determine whether all three *tad* operons are required for its virulence. By deleting each *tad* locus and complementing the deletion *in trans*, we attempted to address these questions (at least in part) and found that all three *tad* operons are required for the full virulence of *V. vulnificus*. Only complete abrogation of all three *tad* loci led to significantly decreased lethality in mice (Table 1). Based on animal and cell culture infection models coupled with molecular genetic analyses, we came

to understand the coordinated contributions of the three *V. vulnificus tad* operons to host cell invasion as well as to survival of complement-mediated bacteriolysis. Deletion of all three *tad* loci impaired the adherence of the bacterial cells to the host cells (Fig 2), thus hampering RtxA1 cytotoxin production and delivery (Fig 5) and, consequently, tissue invasion (Fig 7). These results corroborate our previous findings that host cell contact is required for *V. vulnificus* toxin secretion and pathogenicity [25].

The bactericidal action of serum is an important component of the host defense against bloodstream infections [35, 36]. As most fatal cases of *V. vulnificus* infection result from septicemia, serum resistance is considered an essential feature for survival in the host environment. It is well documented that clinical *V. vulnificus* isolates have a significantly greater survival ability in human serum compared with that of environmental isolates [40, 41]. Several mechanisms have been proposed to explain this phenomenon, the most significant of which may be differences in siderophore expression and/or capsule formation [40]. In the present study, we discovered a novel function of *V. vulnificus* Tad pili in conferring resistance to the complement-mediated bactericidal activity of its host. The ubiquity of the *tad1* cluster in virulent *V. vulnificus* strains suggests that the surface expression of Tad pili may be another key determinant for the survival of *V. vulnificus* in host milieus, which could conceivably differentiate the clinical and environmental strains. Bacteria lacking Tad pili rapidly lost viability in serum via direct complement-mediated bacteriolysis, predominantly activated via the alternative pathway. The mechanism through which Tad pili protect bacteria from complement attack should be further studied. The poor immunogenicity of Flp pili could have something to do with the serum resistance. Given that the *tad* triple mutant lost its slime-like surface morphology (which could be complemented *in trans* by cosmids harboring an individual tad operon), it is plausible that Flp pili could anchor secreted polysaccharides during formation of durable capsular lattice.

Inhibition of the alternative complement pathway by the Flp pili might be related to the low immunogenicity of the structural pilin protein. To understand the poor recognition of Tad pili by the immune system, we analyzed the antigenicity and structural characteristics of Tad pilin using bioinformatics tools. After *in silico* prediction of the 3D structure of Tad pilin, we compared it with the orthologs from *Aggregatibacter actinomycetemcomitans*, which seem to have high functional similarity with that of *V. vulnificus*. *Bordetella pertussis* Fim2 and *Escherichia coli* CfaB (S7 Fig). *V. vulnificus* Tad pilin was predicted to form an alpha helix that partially overlaps structurally with the *A. actinomycetemcomitans* Flp1 and Flp2, which share the Flp common motif [8], and *B. pertussis* Fim2 pilins, which are thought to contribute to the assembly of pilin monomers into the fimbrial ultrastructure. When compared with the immunogenic Fim2 and CfaB pilins, which function as vaccine candidates, Tad pilin appeared to be relatively hydrophobic, and only a small fraction contained the hydrophilicity required for antigenicity (S8 Fig).

The presence of pilus-like structures has been reported to be more closely associated with clinical isolates of *V. vulnificus* than with environmental strains [42]. Under SEM, we observed filamentous surface structures that extended from the wild-type cell bodies that were absent from the Δ*tad123* triple operon mutant cells (Fig 3). Interestingly, the presumable Tad pili structure became more elongated when the cells were grown *in vivo*, suggesting a pathogenic function during establishment of successful infections. This morphological change under *in vivo* culture conditions corroborates the previously suggested hypothesis that the Tad pili significantly contribute to *V. vulnificus* pathogenicity [12]. The thickness and size of the putative pili structures were quite elusive, unlike other Tad/Flp pili such as those of *Aggregatibacter* (previously *Actinobacillus*) [6–9]. To confirm the cell surface expression of Tad pili, we performed immunogold-labeling and fluorescence staining. To the best of our knowledge, no

specific ultrastructural analysis of *V. vulnificus* Tad pili and their molecular pathogenic roles have been previously reported. While performing these experiments, we failed to raise functional antibodies against the *V. vulnificus* Flp pilin, presumably because of its very low hydrophilicity and immunogenicity as addressed above. To overcome this obstacle, we first fused a V5 tag sequence to the N- or C-terminus of the *flp-1* gene on the chromosome. However, we could not detect any signal from chromosomally V5-tagged Flp in a dot blot analysis using an anti-V5 antibody. The V5-tagged Flp might have been structurally defective, leading to ineffective assembly into pili structures. Alternatively, the engineered strains may have incurred polar effects on downstream gene expression during double crossover homologous recombination. We subsequently constructed a V5-tagged Flp overexpression system encoded on the multicopy pBAD24 plasmid (S5 Fig). Our hypothesis was that, when expressed under the control of an arabinose-inducible promoter, some proportion of the overexpressed V5-tagged Flp proteins might be randomly incorporated during assembly of the chromosomally expressed native pilin subunits. As expected, we could detect positive signals from *V. vulnificus* cells overexpressing the Flp-V5 fusion protein in both experiments (Fig 4). However, only a fraction of the transconjugants carrying the overexpression plasmid could be stained with immunogold or fluorescence approaches, suggesting minimal incorporation of V5-tagged Flp expressed from the single-copy chromosomal locus possibly due to structural deformations by addition of the V5 tag.

Taken together, our results provide new insights into the pathogenic significance of Tad pili in *V. vulnificus* CMCP6. The Tad provide pathogenic *V. vulnificus* with the ability to adhere to and invade host cells and shield the cells against complement-mediated bacteriolysis inside the host. During these two distinct stages of infection, the Tad pili-mediated host cell adhesion and evasion of the anti-complement activity inside host provide, respectively, the signal required to induce expression of the potent RtxA1 cytotoxin and the ability of *V. vulnificus* to robustly grow *in vivo*.

Materials and methods

Bacterial strains, plasmids and media

Bacterial strains and plasmids used in this study are listed in Table 2. *V. vulnificus* CMCP6 is a highly virulent clinical isolate from the Chonnam National University Hospital, South Korea [5, 25]. *V. vulnificus* and *E. coli* were grown in 2.5% NaCl heart infusion (HI) and in Luria-Bertani (LB) medium, respectively. Antibiotics were used as previously described [43].

Locus deletion mutant construction and complementation

We constructed in-frame single, double, and triple deletion mutants of entire genes in the *tad1*, *tad2* and *tad3* loci by the allelic-exchange method. We designed two sets of primers to amplify ~1-kb DNA fragments in the upstream or downstream region of each *tad* operon (S1 Table). The primers were synthesized with overhangs recognized by specific restriction enzymes (REs). The upstream and downstream amplicons of each *tad* operon were ligated by cross-over PCR to produce a 2-kb fragment [44]. The fusion fragments were digested with appropriate REs and subcloned into pDM4 suicide vector. The resulting recombinant vector was transformed into *E. coli* SM10 λ *pir* and subsequently transferred into *V. vulnificus* CMCP6 by conjugation. Stable Cm^R transconjugants were selected on *Vibrio*-selective thiosulfate citrate bile salt sucrose (TCBS) agar plate containing Cm. Plating of the transconjugants on 2.5% NaCl HI agar plate containing 10% sucrose was performed to select clones that experienced second homologous recombination events forcing excision of the vector sequence and

Table 2. Strains and plasmids used in this study.

Strain or plasmid	Description	Source or reference
Strains		
V. vulnificus		
CMCP6	Wild-type, clinical isolate	CNU Hospital
Δtad1	CMCP6 with in-frame deletion of entire structural genes in *tad11* locus	This study
Δtad2	CMCP6 with in-frame deletion of entire structural genes in *tad2* locus	This study
Δ tad3	CMCP6 with in-frame deletion of entire structural genes in *tad3* locus	This study
Δ tad12	CMCP6 with in-frame double deletion of entire structural genes in *tad12* loci	This study
Δ tad13	CMCP6 with in-frame double deletion of entire structural genes in *tad13* loci	This study
Δ tad23	CMCP6 with in-frame double deletion of entire structural genes in *tad23* loci	This study
Δ tad123	CMCP6 with in-frame triple deletion of entire structural genes in *tad123* loci	This study
Vv-pBAD	CMCP6 carrying pBAD24 empty vector	This study
Vv-FlpV5	CMCP6 carrying pCMM2103	This study
Δtad-FlpV5	Δtad123 carrying pCMM2103	
E. coli		
BL21 (DE3)	F− *hsdS*(r$_B$− m$_K$−) *gal* with T7 RNA polymerase gene in chromosome	Novagen
DH5α	F⁻ *recA1* restriction negative	Laboratory collection
SY327 λ *pir*	Δ(*lac pro*) *argE* (Am) *rif nalA recA56* λ *pir* lysogen	[52]
SM10 λ *pir*	*thi thr leu tonA lacY supE recA*::RP4-2-Tc^r::Mu Km^r λ *pir* lysogen	[52]
Plasmids		
pBAD24	Expression vector, arabinose inducible promoter; Amp^r	[53]
pET30a$_+$	Km^r *E. coli* cloning vector with T7 promoter upstream of N-terminal His$_6$ tag	Novagen
pDM4	Suicide vector with *oriR6K sacB*; Cm^r	
pLAFR3	IncP cosmid vector; Tc^r	[54]
pRK2013	IncP Km^r Tra Rk2$^+$ *repRK2 repE1*	[55]
pCMM2103	pBAD24 expressing a fusion protein of Flp-1 pilin and V5 tag	This study
pCMM2104	pDM4 with a 2-kb SmaI/XhoI in-frame deleted *tad1* operon	This study
pCMM2105	pDM4 with a 2-kb SmaI/XhoI in-frame deleted *tad2* operon	This study
pCMM2106	pDM4 with a 2-kb SmaI/XhoI in-frame deleted *tad3* operon	This study
pCMM2107	pLAFR3 with a 25-kb fragment containing the in-frame *tad1* operon	This study
pCMM2108	pLAFR3 with a 25-kb fragment containing the in-frame *tad2* operon	This study
pCMM2109	pLAFR3 with a 25-kb fragment containing the in-frame *tad3* operon	This study

Cm^r, chloramphenicol resistance; Tc^r, tetracycline resistance; Amp^r, ampicillin resistance; Km^r, kanamycin resistance.

leaving only mutated or wild-type allele of the genes. Each in-frame deletion mutation was confirmed by PCR with the chromosomal DNA from the respective mutant as template.

For the use in genetic complementation experiments, we screened cosmid clones that contain intact *tad1*, *tad2* or *tad3* operon from a pLAFR3 cosmid library of *V. vulnificus* CMCP6 [25, 45]. The selected cosmid library clone containing an individual *tad* operon was transferred to the triple *tad* operon deletion mutant by triparental mating with a conjugative helper plasmid pRK2013. The transconjugants were screened on TCBS agar plates containing tetracycline

and confirmed by PCR. To fulfill molecular Koch's postulates, we performed a complementation analysis. The Δ*tad123* mutant was separately complemented with an individual cosmid clone harboring each *tad* operon. The restoration of *tad* operon expression was confirmed by the conventional RT-PCR (S4 Fig).

Conventional and real-time RT-PCR

The transcriptional levels of the three structural *flp* genes, which encoded the major structural components of Flp pili, were measured by conventional and real-time RT-PCR. *gyrA* was chosen as the reference gene forn the qRT-PCR as previously reported [45]. Forward and reverse primer pairs were designed and are provided in S2 Table. Total RNA was isolated from log-phase bacterial cells grown in the rat peritoneal cavity or in 2.5% NaCl HI broth using the RNeasy minikit (Qiagen). One microgram of purified RNA was converted into cDNA using QuantiTect Reverse Transcription Kit (Qiagen) in accordance with the manufacturer's protocol. qRT-PCR was performed to quantify each target transcript using QuantiTect SYBR green PCR kit (Qiagen). The relative gene expression was normalized to the expression of *gyrA* using the threshold cycle ($\Delta\Delta C_T$) method [46]. For conventional RT-PCR, 16S rRNA was used as the internal standard. After 25 to 35 cycles, the amplicons were separated on 2% (wt/vol) agarose gels and stained with ethidium bromide. The transcription levels of *flp-1* under iron-limited and solid surface growth conditions were also analyzed by qRT-PCR. For the iron limitation experiment, dipyridyl (Sigma-Aldrich) was added to the 2.5% NaCl HI broth at a final concentration of 80 μM for iron limitation.

Ethics statement

All animal experimental procedures were performed with approval from the Chonnam National University Institutional Animal Care and Use Committee under protocol CNU IACUC-H-2015-44. Animal research facility maintenance and experimental procedures were carried out strictly keeping the guideline in the Animal Welfare Act legislated by Korean Ministry of Agriculture, Food and Rural Affairs.

LD$_{50}$ determination

The intraperitoneal 50% lethal dose (i.p. LD$_{50}$) of *V. vulnificus* was determined using 7-week-old, randomly bred specific-pathogen-free (SPF) female ICR mice (Daehan Animal Co., Daejeon, South Korea). Five mice per group were intraperitoneally inoculated with 10-fold serial dilutions of fresh bacterial suspensions (10^9 to 10^5 CFU/mouse). The intragastric (i.g.) LD$_{50}$ was determined using six-day-old randomly bred SPF CD-1 suckling mice (Daehan Animal Co., Daejeon, South Korea). Seven mice per group were intragastrically administered with 10-fold serial dilutions of fresh bacterial suspensions containing 0.1% Evans blue (Sigma-Aldrich) to ensure correct i.g. administration. The control animals received 100 μl of PBS containing 0.1% Evans Blue. The challenged mice were monitored for 48 h. LD$_{50}$ values were calculated based on probit analysis, using IBM SPSS 21.0 software (IBM).

Construction of C-terminally V5-tagged Flp (Flp-V5)

DNA fragments of the structural *flp-1* pilus gene without its stop codon were amplified and subcloned into the pBAD24 vector. Subsequently, double-stranded oligonucleotides encoding the V5 peptide, "GGTAAGCCTATCCCTAACCCTCTCCTCGGTCTCGATTCTACGTAA", were fused to the C-terminus of the *flp-1* gene in the pBAD24-Flp plasmid. At the end of the V5 sequence, a TAA codon was added to terminate translation. The pBAD24 plasmids containing

the Flp-V5 fusion protein were transformed into *E. coli* DH5α competent cell. The sequence of the cloned fragment was confirmed by DNA sequencing. The resulting vectors were transferred into *V. vulnificus* via triparental mating with a conjugative helper plasmid pRK2013. The trans-conjugants were screened on 2.5% NaCl HI agar plates containing ampicillin.

Dot blot analysis

V. vulnificus strains carrying pCMM2103 (pBAD24::Flp-V5) were grown for 4 h on 2.5% NaCl HI agar plates containing ampicillin. Flp-V5 expression was induced for 4 h via addition of 0.1% L-arabinose. The cell suspensions were applied to nitrocellulose membrane and fixed with 4% paraformaldehyde for 20 min. The membrane was blocked for 1 h using 5% skim milk in PBS and then incubated with anti-V5 polyclonal antibodies (diluted 1:5000, Abcam) for 2 h. After washing, the membrane was developed with HRP-conjugated goat anti-rabbit IgG secondary antibody (Dako). Stained dots on a white background indicated positive results.

Scanning electron microscopy

To compare surface structure of the wild-type, Δ*tad123* and Δ*tad123* (pLAFR3::*tad1*), we performed SEM observation. Bacteria were grown *in vivo* using a rat peritoneal infection model as previously described [45]. To minimize shearing force during bacterial preparations, all procedures were carefully performed. And we also applied osmotic adaptation with fixative by 3 staged applying a step-down approach from 2.5% NaCl containing fixative to 0.9% and 0% NaCl containing solution with a gentle agitation. Bacterial cells were fixed at room temperature for 4 h in a fixation solution containing 0.5% glutaraldehyde and 4% paraformaldehyde in 0.05 M sodium cacodylate buffer (pH 7.2). After three washes with 0.05 M cacodylate buffer, all of the samples were mounted on nickel grids coated with carbon film (150 mesh) (EMS, USA). After blocking nonspecific binding sites with 1% BSA in EM-immunogold (EMG) buffer (0.05% Tween, 0.5 M NaCl, 0.01 M phosphate buffer, pH 7.2), the samples were incubated at 4°C for 24 h with anti-V5 tag monoclonal antibody (ab27671, Abcam, UK) at a 1:20 dilution at 4°C, followed with incubation for 1 h in goat anti-rat antibody (1:50) conjugated to 6 nm gold particles. The grids were washed in EMG buffer, PBS, and distilled water and stained for 12 min with 4% uranyl acetate in deionized distilled water. The surfaces of all of the samples were observed using a field emission scanning electron microscope (Helios G3 CX, FEI Co., Hillsboro, Oregon, USA) at 1 kV acceleration with TED mode.

Immunogold labellng

A drop of *V. vulnificus* cell suspension was applied to a nickel grid coated with carbon film for 1 min. Because of its structural fragility of *V. vulnificus*, we prepared the bacterial sample with very gentle manner such as limited frequencies of pipetting and washing processes. Moreover, to minimize the insults from the critical points drying, we firstly fixed the *in vivo* grown cells with osmolarity-modified fixative (which contains 2.5% NaCl) and changed the solution to conventional fixative for SEM study (0.5% glutaraldehyde and 4% paraformaldehyde in 0.05 M sodium cacodylate buffer (pH 7.2)) under room temperature. Moreover, to reduce damages from electron and enhance the resolution beam during SEM analysis, we used the focused ion scanning electron microscope (FIB). Subsequently, the samples were incubated with the anti-V5 polyclonal antibody (diluted 1:20, Abcam) and labeled with 5-nm colloidal gold-conjugated goat anti-rabbit IgG secondary antibody (diluted 1:20, BritishBio-Cell, UK).

Transmission electron microscopy

V. vulnificus cells were fixed in a fixation solution containing 0.5% glutaraldehyde and 4% paraformaldehyde in 0.05 M sodium cacodylate buffer (pH 7.2) at room temperature for 4 h. After three washes with 0.05 M cacodylate buffer, all of the samples were mounted on nickel grids coated with carbon film (150 mesh) (EMS, USA). After staining with 2% uranyl acetate, the samples were examined with a transmission electron microscope (TEM) (JEM-1400; JEOL Ltd., Japan) at 80 kV acceleration. For quantification and statistical analysis of immunogold-conjugated observation by EM, we counted gold particles in obtained EM photos. To get objective results, three different researchers independently counted gold dots associated with 5 bacterial images under x10,000 magnification field.

Confocal microscopy

To induce V5-tagged pilin expression, mid-log phase *V. vulnificus* cells were grown for 4 h on 2.5% NaCl HI-ampicillin agar plates supplemented with 0.1% L-arabinose. Bacterial pellet was then gently suspended in PBS buffer. The induced bacterial cells were directly immobilized on poly-L-lysine-coated coverslips. Samples were fixed with 4% formaldehyde for 30 min and then incubated with primary anti-V5 antibodies (1:300) for 2 h. After three washes with PBS buffer, the cells were incubated for 1 h with a Texas Red-conjugated anti-rabbit secondary antibody (Molecular Probes) and DAPI (Invitrogen). The samples were observed under a laser scanning confocal microscope (LSM 510, Zeiss, Oberkochen, Germany), and the obtained images were analyzed by using the ZEN Lite software (Zeiss, Oberkochen, Germany).

Adhesion assay

We quantitatively analyzed bacterial adhesion to host cell by using viable cell counting and microscopic observation. HeLa cell monolayers (5×10^5/well) were grown on 24 well plates (SPL, cat#30024) and then infected for 45 minutes with log-phase *V. vulnificus* cells at MOI 250. The monolayer was washed twice with PBS to remove non-adherent bacteria. The wells were then suspended with 200 μl of PBS containing 0.1% Triton and incubated for 10 minutes at room temperature. The number of colony forming units (CFU) that adhered to Hela cells was enumerated by ten fold serially diluting in PBS and spotted on HI agar plates.

For microscopic observation, the cells were fixed in methanol after the PBS washing and stained with 0.1% Giemsa solution (Sigma-Aldrich). The number of *V. vulnificus* cells that adhered to single HeLa cells was counted under a light microscope at 400× and 1,000× magnification (Nikon Eclipse 50i, Japan).

Determination of biofilm and confocal imaging

To induce the biofilm formation, freshly cultured *V. vulnificus* cells (5×10^5 CFU/ml) were applied into each well of 24 well plates (SPL, cat#30024). The plates were further incubated at 37˚C for 24 hours and then gently washed once with PBS. The wells were stained with 200 μl of 0.3% crystal violet for 15 minutes and gently washed with PBS. The stained biofilm was extracted with 200 μl of 100% ethanol and two fold diluted with PBS to measure the absorbance at 595 nm by a microplate reader (Molecular Devices Corp., Menlo Park, CA). To acquire the confocal microscopic images of biofilm, the biofilm was induced in 4 Well Cell Culture Slide (SPL, cat#30124) for 24 hours and then gently washed once with PBS. The biofilm was then stained with acridine orange and observed by a confocal microscope as previously reported [47]. The samples were observed under a LSM510 confocal microscope (Zeiss,

Oberkochen, Germany), and the obtained images were analyzed by using the ZEN 2012 x32 blue software.

Western blot analysis

To detect RtxA1, HeLa cells grown in 6-well plates were infected for 35 and 45 min with log-phase *V. vulnificus* strains at an MOI of 100. The bacteria attached to the HeLa cells were lysed using a lysis buffer (Cell Signaling), followed by concentration using an Amicon Ultra-0.5 centrifugal filter apparatus (Merck KgaA). The samples were then subjected to 10% SDS-PAGE. RtxA1 proteins were detected using an anti-GD domain antibody (RtxA1-C, a band of approximately 130 kDa) [30].

Cytotoxicity assay

To determine the effect of *tad* operon mutations on cytotoxicity against HeLa cells, we performed the lactate dehydrogenase (LDH) release assay as previously described [43].

In vivo invasion assay

Bacterial cells that translocated from the intestine to the bloodstream were measured as previously described [48]. Seven-week-old randomly bred SPF female ICR mice were starved for 16 h. The ileum was tied off in a 5-cm segment and log-phase *V. vulnificus* cells (4.0×10^6 CFU/ 400 μl) were inoculated into the ligated segment. Blood samples were acquired from the infected mice via cardiac puncture. The number of viable bacterial cells was counted by plating on 2.5% NaCl HI agar plates. In parallel, viable *V. vulnificus* cells in the ligated ileal loops were also enumerated by plating on TCBS agar plates.

In vitro invasion assay

Polarized HCA-7 cells grown in Transwell filter chambers (8 μm pore size; CoStar, Cambridge, MA, USA) were apically exposed to log-phase *V. vulnificus* cells at an MOI of 5. Invasiveness was determined by measuring the number of bacterial cells that translocated from the apical to basolateral compartment of the Transwells. Viable bacterial cells were counted by plating on 2.5% NaCl HI agar plates.

Determination of *in vivo V. vulnificus* growth

In vivo growth of *V. vulnificus* was measured using the dialysis tube implantation model as previously described [48]. CelluSep H1 dialysis tubing (MWCO 12,000~14,000; Membrane Filtration Products, Inc. Texas) was incubated with PBS overnight. The dialysis tube was disinfected with 70% alcohol for 1 h and washed three times with sterile PBS before use. Seven-week-old female Sprague Dawley (SD) rats (DBL. Co. Ltd, Daejeon, Korea) were anesthetized with a mixture of 10% Zoletil and 5% Rumpun dissolved in PBS. Three 10-cm dialysis tubes containing 2 ml of 5×10^5 CFU/ml *V. vulnificus* cells were surgically implanted into the rat peritoneal cavity. The bacterial growth at each time point was analyzed using three rats. Culture samples were harvested for viable cell counting on 2.5% NaCl HI agar plates 2, 4 and 6 h after implantation.

V. vulnificus growth in mouse blood

To assess bacterial growth in blood, seven mice per group were intravenously (i.v.) or i.p. injected with 100 μl of 5×10^5 CFU cells that had been incubated in the rat peritoneal cavity for 6 h for induction of *tad1* locus expression and *in vivo* adaptation. Blood samples were

acquired from the infected mice via cardiac puncture at the indicated times. Viable bacterial cells were counted by plating on 2.5% NaCl HI agar plates.

Determination of serum bactericidal activity against *V. vulnificus*

Log-phase *V. vulnificus* cells (1.0×10^7 CFU/10 μl) were added to 200 μl of PBS containing various NHS concentrations. The samples were incubated at 37°C for appropriate times. Viable bacterial cells were counted by plating on 2.5% NaCl HI agar plates. To block activation of the classical pathway, NHS was pretreated with 10 mM ethylene glycol-bis (2-aminoethylether)-*N*, *N*, *N′*, *N′*-tetraacetic acid and 5 mM $MgCl_2$ for 30 min at 37°C (EGTA/Mg^{2+}) [49]. To prepare the MBL-depleted serum, mannose-agarose beads (Sigma-Aldrich) were washed three times with sterile PBS and then incubated with NHS at 4°C for 1 h with gentle rotation [50]. The alternative pathway is inhibited via properdin absorption with bentonite [51]. 10 mg of bentonite was washed three times with PBS and incubated with NHS at 37°C for 10 min to absorb the properdin.

Anti-C5 pretreatment and determination of *V. vulnificus* in bloodstream

Seven-week-old randomly bred SPF female ICR mice were intraperitoneally administered with 40 mg/kg/day of anti-C5 monoclonal antibody (Hycult BiotechInc, Pa, USA) or isotype control two times in two-days interval following manufacturer's instruction. Twenty-four hours after the second administration of the anti-C5, mice were intraperitoneally infected with 5×10^5 CFU cells that had been incubated in the rat peritoneal cavity for 6 h for *in vivo* adaptation. Blood samples were acquired from the infected mice by eye puncture in a time course. Viable bacterial cells were counted by plating on 2.5% NaCl HI agar plates.

Statistical analysis

The results are expressed as the mean ± standard error of the mean (SEM) unless otherwise stated. Each experiment was repeated a minimum of three times, and the results from representative experiments are shown. Statistical analyses were performed using the Prism 6.00 software for Windows (GraphPad software, San Diego, CA). Multiple comparisons were performed using Student's *t* test and analysis of variance (ANOVA) followed by Bonferroni *post hoc* tests. *P*-values < 0.05 was considered statistically significant.

Supporting information

S1 Fig. *Vibrio vulnificus* CMCP6 *tad* loci.
(PPTX)

S2 Fig. Significantly prolonged survival of mice intraperitoneally infected with the Δ*tad123* mutant strain (n = 5). Seven-week-old randomly bred SPF female ICR mice were intraperitoneally infected with 1×10^7 CFU/mouse **(A)** or 1×10^6 CFU/mouse **(B)** of fresh bacterial suspensions. The challenged mice were monitored for 48 h. Statistical analysis was carried out using Kaplan-Meier analysis followed by the log-rank test (**, *P* < 0.01).
(PPTX)

S3 Fig. Effects of Tad operon mutations on the adhesion to host cells (A), cytotoxicity (B), biofilm formation (C), *in vitro* invasion (D), and human serum susceptibility (E). Log-phase bacteria were used for the experiments.
(PPTX)

S4 Fig. Restoration of structural *flp* gene expression in *tad* operon-complemented strains.
(A) Expression of the structural *flp* genes was assessed using conventional RT-PCR. RNA was isolated from log-phase bacteria grown in 2.5% NaCl HI broth and then converted into cDNA. RT-PCR was performed using primers specific for each structural *flp* gene as shown in S2 Table. The 16S *rRNA* housekeeping gene was employed as the internal control. (B) Bacterial growth in 2.5 HI broth.
(PPTX)

S5 Fig. Detection of V5-tagged Flp fusion proteins from induced *E. coli* cells by Western blot analysis. Bacteria were grown in LB Amp broth supplemented with (inducing) or without (non-inducing) 0.1% arabinose for 4 h. The Flp-V5 fusion proteins were detected using an anti-V5 polyclonal antibody.
(PPTX)

S6 Fig. Growth of *V. vulnificus* in high-glucose DMEM. Log-phase *V. vulnificus* cells were grown in high-glucose DMEM, and the OD_{600} was measured every two hours for 8 h. The growth pattern of the $\Delta tad123$ mutant cells was identical to that of the wild-type strain. Data shown represent the mean ± SEM of three independent experiments performed in triplicate.
(PPTX)

S7 Fig. Comparison of *V. vulnificus tad* with other bacterial pilins. The predicted 3D structure of *V. vulnificus* Tad pilin (hot pink) was overlaid with those of *A. actinomycetemcomitans* Flp1 **(A, yellow)** and Flp2 **(B, orange)**, *B. pertussis* Fim2 **(C, cyan)**, and *E. coli* CfaB **(D, green)**. The structures were simulated with the Protein Homology/analogY Recognition Engine V 2.0 (http://www.sbg.bio.ic.ac.uk/phyre2/html/page.cgi?id=index) and superimposed using the MacPyMol version 1.7.4 Education License.
(PPTX)

S8 Fig. Hydrophilicity comparison of *V. vulnificus* Tad pilin (red) with immunogenic *B. pertussis* Fim2 (blue) and *E. coli* CfaB (green). Positive values indicate hydrophilicity while negative values indicate hydrophobicity. The red line shows the average (Avg) hydrophilicity scores of the Fim2 and CfaB antigenic domains, calculated value of which was -0.04. Only a minor fraction adjacent to the alpha helical region of Tad pilin showed positive hydrophilicity but remained lower than 0.5 hydrophilicity.
(PPTX)

S1 Table. Primers used for the construction of *tad* operon deletion mutants and the fusion protein.
(DOCX)

S2 Table. Primers used in the RT-PCR study.
(DOCX)

Acknowledgments

Author Contributions

Conceptualization: Shee Eun Lee, Joon Haeng Rhee.

Data curation: Tra-My Duong-Nu, Kwangjoon Jeong, Sao Puth, Soo Young Kim, Wenzhi Tan, Joon Haeng Rhee.

Formal analysis: Tra-My Duong-Nu, Sao Puth, Soo Young Kim, Wenzhi Tan, Shee Eun Lee, Joon Haeng Rhee.

Funding acquisition: Shee Eun Lee, Joon Haeng Rhee.

Investigation: Tra-My Duong-Nu, Seol Hee Hong, Sao Puth, Soo Young Kim, Wenzhi Tan, Shee Eun Lee.

Methodology: Tra-My Duong-Nu, Kwangjoon Jeong, Seol Hee Hong.

Project administration: Joon Haeng Rhee.

Resources: Kwangjoon Jeong, Shee Eun Lee, Joon Haeng Rhee.

Software: Tra-My Duong-Nu, Kwangjoon Jeong.

Supervision: Shee Eun Lee, Joon Haeng Rhee.

Validation: Tra-My Duong-Nu, Kwangjoon Jeong, Sao Puth, Soo Young Kim, Wenzhi Tan, Kwang Ho Lee, Shee Eun Lee, Joon Haeng Rhee.

Visualization: Tra-My Duong-Nu, Kwangjoon Jeong, Kwang Ho Lee.

Writing – original draft: Tra-My Duong-Nu, Kwangjoon Jeong, Shee Eun Lee, Joon Haeng Rhee.

Writing – review & editing: Shee Eun Lee, Joon Haeng Rhee.

References

1. Klontz KC, Lieb S, Schreiber M, Janowski HT, Baldy LM, Gunn RA. Syndromes of *Vibrio vulnificus* infections: clinical and epidemiologic features in Florida cases, 1981–1987. Annals of Internal Medicine. 1988; 109(4):318–23. https://doi.org/10.7326/0003-4819-109-4-318 PMID: 3260760

2. Hlady WG, Klontz KC. The epidemiology of *Vibrio* infections in Florida, 1981–1993. Journal of Infectious Diseases. 1996; 173(5):1176–83. https://doi.org/10.1093/infdis/173.5.1176 PMID: 8627070

3. Shapiro RL, Altekruse S, Hutwagner L, Bishop R, Hammond R, Wilson S, et al. The role of gulf coast oysters harvested in warmer months in *Vibrio vulnificus* infections in the United States, 1988–1996. J Infect Dis. 1998; 178(3):752–9. https://doi.org/10.1086/515367 PMID: 9728544

4. Michael HB, Kathleen S, Robert M, Rayford BM. *Vibrio vulnificus* Infection: diagnosis and treatment. Am Fam Physician 2007; 76(4):539–44. PMID: 17853628

5. Kim YR, Lee SE, Kim CM, Kim SY, Shin EK, Shin DH, et al. Characterization and Pathogenic Significance of Vibrio vulnificus Antigens Preferentially Expressed in Septicemic Patients. Infection and . . . . 2003; 71(10):5461–71. https://doi.org/10.1128/IAI.71.10.5461-5471.2003 PMID: 14500463

6. Kachlany SC, Planet PJ, Bhattacharjee MK, Kollia E, DeSalle R, Fine DH, et al. Nonspecific adherence by *Actinobacillus actinomycetemcomitans* requires genes widespread in bacteria and archaea. Journal of Bacteriology. 2000; 182(21):6169–76. https://doi.org/10.1128/jb.182.21.6169-6176.2000 PMID: 11029439

7. Kachlany SC, Planet PJ, DeSalle R, Fine DH, Figurski DH. Genes for tight adherence of *Actinobacillus actinomycetemcomitans*: from plaque to plague to pond scum. Trends in Microbiology. 2001; 9(9):429–37. https://doi.org/10.1016/S0966-842X(01)02161-8. PMID: 11553455

8. Kachlany SC, Planet PJ, DeSalle R, Fine DH, Figurski DH, Kaplan JB. *flp-1*, the first representative of a new pilin gene subfamily, is required for non-specific adherence of *Actinobacillus actinomycetemcomitans*. Molecular Microbiology. 2001; 40(3):542–54. https://doi.org/10.1046/j.1365-2958.2001.02422.x PMID: 11359562

9. Planet PJ, Kachlany SC, Fine DH, DeSalle R, Figurski DH. The widespread colonization island of *Actinobacillus actinomycetemcomitans*. Nat Genet. 2003; 34(2):193–8. https://doi.org/10.1038/ng1154 PMID: 12717435

10. Spinola SM, Fortney KR, Katz BP, Latimer JL, Mock JR, Vakevainen M, et al. *Haemophilus ducreyi* requires an intact *flp* gene cluster for virulence in humans. Infection and Immunity. 2003; 71(12):7178–82. https://doi.org/10.1128/IAI.71.12.7178-7182.2003 PMID: 14638812

11. De Bentzmann S, Aurouze M, Ball G, Filloux A. FppA, a novel *Pseudomonas aeruginosa* prepilin peptidase involved in assembly of type IVb pili. Journal of Bacteriology. 2006; 188(13):4851–60. https://doi.org/10.1128/JB.00345-06 PMID: 16788194

12. Pu M, Rowe-Magnus DA. A Tad pilus promotes the establishment and resistance of Vibrio vulnificus biofilms to mechanical clearance. NPJ Biofilms Microbiomes. 2018; 4:10. https://doi.org/10.1038/s41522-018-0052-7 PMID: 29707230

13. Waldor MK, Mekalanos JJ. Lysogenic conversion by a filamentous phage encoding cholera toxin. Science. 1996; 272(5270):1910–4. Epub 1996/06/28. https://doi.org/10.1126/science.272.5270.1910 PMID: 8658163.

14. Li J, Lim MS, Li S, Brock M, Pique ME, Woods VL Jr., et al. Vibrio cholerae toxin-coregulated pilus structure analyzed by hydrogen/deuterium exchange mass spectrometry. Structure. 2008; 16(1):137–48. Epub 2008/01/11. https://doi.org/10.1016/j.str.2007.10.027 PMID: 18184591

15. Kirn TJ, Lafferty MJ, Sandoe CM, Taylor RK. Delineation of pilin domains required for bacterial association into microcolonies and intestinal colonization by Vibrio cholerae. Mol Microbiol. 2000; 35(4):896–910. Epub 2000/02/26. https://doi.org/10.1046/j.1365-2958.2000.01764.x PMID: 10692166.

16. Tomich M, Planet PJ, Figurski DH. The tad locus: postcards from the widespread colonization island. Nature Reviews Microbiology. 2007; 5(5):363–75. https://doi.org/10.1038/nrmicro1636 PMID: 17435791

17. Pu M, Duriez P, Arazi M, Rowe-Magnus DA. A conserved tad pilus promotes Vibrio vulnificus oyster colonization. Environ Microbiol. 2018; 20(2):828–41. Epub 2017/12/14. https://doi.org/10.1111/1462-2920.14025 PMID: 29235706.

18. Alice AF, Naka H, Crosa JH. Global gene expression as a function of the iron status of the bacterial cell: influence of differentially expressed genes in the virulence of the human pathogen *Vibrio vulnificus*. Infection and Immunity. 2008; 76(9):4019–37. https://doi.org/10.1128/IAI.00208-08 PMID: 18573903

19. Gulig PA, Crécy-Lagard Vd, Wright AC, Walts B, Telonis-Scott M, McIntyre LM. SOLiD sequencing of four *Vibrio vulnificus* genomes enables comparative genomic analysis and identification of candidate clade-specific virulence genes. BMC Genomics. 2010; 11:512-. https://doi.org/10.1186/1471-2164-11-512 PMID: 20863407

20. Morrison SS, Williams T, Cain A, Froelich B, Taylor C, Baker-Austin C, et al. Pyrosequencing-based comparative genome analysis of *Vibrio vulnificus* environmental isolates. PLoS ONE. 2012; 7(5): e37553. https://doi.org/10.1371/journal.pone.0037553 PMID: 22662170

21. Bisharat N, Bronstein M, Korner M, Schnitzer T, Koton Y. Transcriptome profiling analysis of *Vibrio vulnificus* during human infection. Microbiology. 2013; 159:1878–87. https://doi.org/10.1099/mic.0.067900-0 PMID: 23782800

22. Williams TC, Blackman ER, Morrison SS, Gibas CJ, Oliver JD. Transcriptome sequencing reveals the virulence and environmental genetic programs of Vibrio vulnificus exposed to host and estuarine conditions. PloS one. 2014; 9(12):e114376–e. https://doi.org/10.1371/journal.pone.0114376 PMID: 25489854.

23. Kuchma SL, Griffin EF, O'Toole GA. Minor pilins of the type IV pilus system participate in the negative regulation of swarming motility. Journal of Bacteriology. 2012; 194(19):5388–403. https://doi.org/10.1128/JB.00899-12 PMID: 22865844

24. Cowles KN, Gitai Z. Surface association and the MreB cytoskeleton regulate pilus production, localization, and function in *Pseudomonas aeruginosa*. Molecular microbiology. 2010; 76(6):1411–26. https://doi.org/10.1111/j.1365-2958.2010.07132.x PMID: 20398206

25. Kim YR, Lee SE, Kook H, Yeom JA, Na HS, Kim SY, et al. Vibrio vulnificus RTX toxin kills host cells only after contact of the bacteria with host cells. Cellular Microbiology. 2008; 10(4):848–62. https://doi.org/10.1111/j.1462-5822.2007.01088.x PMID: 18005241.

26. Hor LI, Chen CL. Cytotoxins of *Vibrio vulnificus*: functions and roles in pathogenesis. BioMedicine. 2013; 3(1):19–26. http://dx.doi.org/10.1016/j.biomed.2012.12.003.

27. Jeong HG, Satchell KJF. Additive function of *Vibrio vulnificus* MARTX(Vv) and VvhA cytolysins promotes rapid growth and epithelial tissue necrosis during intestinal infection. PLoS Pathogens. 2012; 8 (3):e1002581. https://doi.org/10.1371/journal.ppat.1002581 PMID: 22457618

28. Lo HR, Lin JH, Chen YH, Chen CL, Shao CP, Lai YC, et al. RTX toxin enhances the survival of *Vibrio vulnificus* during infection by protecting the organism from phagocytosis. Journal of Infectious Diseases. 2011; 203(12):1866–74. https://doi.org/10.1093/infdis/jir070 PMID: 21422475

29. Wright AC, Morris JG. The extracellular cytolysin of *Vibrio vulnificus*: inactivation and relationship to virulence in mice. Infection and Immunity. 1991; 59(1):192–7. PMID: 1846124

30. Kim YR, Lee SE, Kang IC, Nam KI, Choy HE, Rhee JH. A bacterial RTX toxin causes programmed necrotic cell death through calcium-mediated mitochondrial dysfunction. J Infect Dis. 2013; 207 (9):1406–15. https://doi.org/10.1093/infdis/jis746 PMID: 23225896

31. Angelov A, Bergen P, Nadler F, Hornburg P. Novel Flp pilus biogenesis-dependent natural transformation. Frontiers in . . .. 2015.

32. Giltner CL, Nguyen Y, Burrows LL. Type IV pilin proteins: versatile molecular modules. Microbiology and molecular biology reviews: MMBR. 2012; 76(4):740–72.

33. Maier B, Wong GCL. How Bacteria Use Type IV Pili Machinery on Surfaces. Trends in Microbiology. 2015; 23(12):775–88. https://doi.org/10.1016/j.tim.2015.09.002 PMID: 26497940

34. Nykyri J, Mattinen L, Niemi O, Adhikari S, Kõiv V, Somervuo P, et al. Role and Regulation of the Flp/Tad Pilus in the Virulence of Pectobacterium atrosepticum SCRI1043 and Pectobacterium wasabiae SCC3193. PLoS ONE. 2013; 8(9):e73718–11. https://doi.org/10.1371/journal.pone.0073718 PMID: 24040039

35. Walport MJ. Complement. New England Journal of Medicine. 2001; 344(14):1058–66. https://doi.org/10.1056/NEJM200104053441406 PMID: 11287977.

36. Frank MM, Joiner K, Hammer C. The function of antibody and complement in the lysis of bacteria. Rev Infect Dis. 1987; 9(Supplement_5):S537–S45. https://doi.org/10.1093/clinids/9.Supplement_5.S537

37. Blom AM, Hallström T, Riesbeck K. Complement evasion strategies of pathogens—Acquisition of inhibitors and beyond. Molecular Immunology. 2009; 46(14):2808–17. https://doi.org/10.1016/j.molimm.2009.04.025. PMID: 19477524

38. Lappegard KT, Bjerre A, Tjonnfjord GE, Mollnes TE. Therapeutic complement inhibition—from experimental to clinical medicine. Tidsskr Nor Laegeforen. 2015; 135(19):1745–9. https://doi.org/10.4045/tidsskr.15.0049 PMID: 26486669.

39. Ong GL, Mattes MJ. Mouse strains with typical mammalian levels of complement activity. J Immunol Methods. 1989; 125(1–2):147–58. Epub 1989/12/20. https://doi.org/10.1016/0022-1759(89)90088-4 PMID: 2607149.

40. Bogard RW, Oliver JD. Role of iron in human serum resistance of the clinical and environmental *Vibrio vulnificus* genotypes. Applied and Environmental Microbiology. 2007; 73(23):7501–5. https://doi.org/10.1128/AEM.01551-07 PMID: 17933938

41. Williams TC, Ayrapetyan M, Ryan H, Oliver JD. Serum survival of *Vibrio vulnificus*: Role of genotype, capsule, complement, clinical origin, and in situ incubation. Pathogens. 2014; 3(4):822–32. https://doi.org/10.3390/pathogens3040822 PMID: 25436506

42. Gander RM, LaRocco MT. Detection of pilus-like structures on clinical and environmental isolates of *Vibrio vulnificus*. Journal of Clinical Microbiology. 1989; 27(5):1015–21. PMID: 2568368

43. Wenzhi Tan, Vivek Verma, K J, Kim SY, Jung CH, Lee SE, et al. Molecular characterization of vulnibactin biosynthesis in *Vibrio vulnificus* indicates the existence of an alternative siderophore. Frontiers in Microbiology. 2014; 5. https://doi.org/10.3389/fmicb.2014.00001 PMID: 24478763

44. Horton RM, Hunt HD, Ho SN, Pullen JK, Pease LR. Engineering hybrid genes without the use of restriction enzymes: gene splicing by overlap extension. Gene. 1989; 77(1):61–8. http://dx.doi.org/10.1016/0378-1119(89)90359-4 PMID: 2744488

45. Duong-Nu T-M, Jeong K, Hong SH, Nguyen H-V, Ngo V-H, Min J-J, et al. All Three TonB Systems Are Required for Vibrio vulnificus CMCP6 Tissue Invasiveness by Controlling Flagellum Expression. Infection and Immunity. 2015; 84(1):254–65. Epub 2nd ed. https://doi.org/10.1128/IAI.00821-15 PMID: 26527216

46. Livak KJ, Schmittgen TD. Analysis of relative gene expression data using real-time quantitative PCR and the 2−ΔΔCT method. Methods. 2001; 25(4):402–8. http://dx.doi.org/10.1006/meth.2001.1262. PMID: 11846609

47. Puth S, Hong SH, Na HS, Lee HH, Lee YS, Kim SY, et al. A built-in adjuvant-engineered mucosal vaccine against dysbiotic periodontal diseases. Mucosal Immunol. 2019; 12(2):565–79. Epub 2018/11/30. https://doi.org/10.1038/s41385-018-0104-6 PMID: 30487648.

48. Duong-Nu TM, Jeong KJ, Hong SH, Min JJ, Lee SE, Rhee JH. All three TonB systems are required for *Vibrio vulnificus* CMCP6 tissue invasiveness by controlling flagellum expression. Infection and Immunity. 2015. https://doi.org/10.1128/iai.00821-15 PMID: 26527216

49. Fine DP, Marney SR, Colley DG, Sergent JS, Des Prez RM. C3 shunt activation in human serum chelated with EGTA. The Journal of Immunology. 1972; 109(4):807–9. PMID: 4627510

50. Aung KM, Sjöström AE, Von Pawel-Rammingen U, Riesbeck K, Uhlin BE, Wai SN. Naturally occurring IgG antibodies provide innate protection against *Vibrio cholerae* bacteremia by recognition of the outer membrane protein U. Journal of Innate Immunity. 2016; 8(3):269–83. https://doi.org/10.1159/000443646 PMID: 26934383

51. Liu YF, Yan JJ, Lei HY, Teng CH, Wang MC, Tseng CC, et al. Loss of outer membrane protein C in *Escherichia coli* contributes to both antibiotic resistance and escaping antibody-dependent bactericidal activity. Infection and Immunity. 2012; 80(5):1815–22. https://doi.org/10.1128/IAI.06395-11 PMID: 22354022

52. Miller VL, Mekalanos JJ. A novel suicide vector and its use in construction of insertion mutations: osmo-regulation of outer membrane proteins and virulence determinants in *Vibrio cholerae* requires ToxR. Journal of Bacteriology. 1988; 170(6):2575–83. https://doi.org/10.1128/jb.170.6.2575-2583.1988 PMID: 2836362

53. Guzman LM, Belin D, Carson MJ, Beckwith J. Tight regulation, modulation, and high-level expression by vectors containing the arabinose PBAD promoter. Journal of Bacteriology. 1995; 177(14):4121–30. https://doi.org/10.1128/jb.177.14.4121-4130.1995 PMID: 7608087

54. Staskawicz B, Dahlbeck D, Keen N, Napoli C. Molecular characterization of cloned avirulence genes from race 0 and race 1 of *Pseudomonas syringae pv. glycinea*. Journal of Bacteriology. 1987; 169 (12):5789–94. https://doi.org/10.1128/jb.169.12.5789-5794.1987 PMID: 2824447

55. Ditta G, Stanfield S, Corbin D, Helinski DR. Broad host range DNA cloning system for Gram-negative bacteria: construction of a gene bank of *Rhizobium meliloti*. Proc Natl Acad Sci U S A. 1980; 77 (12):7347–51. https://doi.org/10.1073/pnas.77.12.7347 PMID: 7012838.